Three-dimensional Electron Microscopy Analysis Reveals Endopolygeny-like Nuclear Architecture Segregation in *Plasmodium* Oocyst Development

A Dissertation Submitted to

the Graduate School of Life and Environmental Sciences,

the University of Tsukuba

in Partial Fulfillment of the Requirements

for the Degree of Doctor of Philosophy in Science

Doctoral Program in Biological sciences

Tamasa ARAKI

Table of contents

Abstract 1

Chapter 1.
General Introduction
1-1 Malaria 2
1-2 Eukaryotic cell division 2
1-3 Life cycle of the malaria parasite 3
1-4 The electron microscopy analysis of the *Plasmodium* 4
1-5 The diversity of cell division in Apicomplexan parasites 4

Chapter 2.
Morphological differences between malaria parasites in oocyst stage development by 2D-SEM
2-1 Abstract 6
2-2 Introduction 6
2-3 Materials and methods
2-3-1 Animal experiments and ethical committees 6
2-3-2 Parasites and reporter parasites used 7
2-3-3 Mosquito experiments for oocyst sample preparation 7
2-3-4 Sample preparation for SEM 8
2-4 Results
2-4-1 Morphological differences between rodent malaria parasites in oocyst stage development 9
2-4-2 The protruding oocyst with a smooth membrane appearance was connected to the mosquito basal membrane in *P. cynomolgi* 10
2-4-3 Evaluation of oocyst diameter size and flat area in each *Plasmodium parasites* 10
2-5 Discussion 10
2-6 Figure Legends 11
2-7 Figures and table 12

Chapter 3.
The 3D-structural reconstruction of sporozoites using classical array tomography
3-1 Abstract 15
3-2 Introduction 15

3-3 Materials and methods
3-3-1 Reporter parasites used . . . 15
3-3-2 Mosquito experiments for SPZ sample preparation . . . 16
3-3-3 TEM and classical 3D analysis . . . 16
3-4 Results
3-4-1 The majority of Pb-SPZ accumulation was observed in the epithelial cells of SG lateral lobes . . . 17
3-4-2 Rodent malaria parasites in the SG, the quality of organelle resolution was insufficient by classical 3D structure analysis . . . 17
3-5 Discussion . . . 18
3-6 Figure legends . . . 19
3-7 Figures . . . 20

Chapter 4.
Three-dimensional FIB-SEM analysis of the organelle segregation in *Plasmodium* oocyst development
4-1 Abstract . . . 22
4-2 Introduction . . . 22
4-3 Materials and methods
4-3-1 Animal experiments and ethical committees . . . 23
4-3-2 Parasites and reporter parasite used . . . 23
4-3-3 Generation of transgenic *Pb* line *Pb*SAS6-$_{mChcon}$ . . . 24
4-3-4 Mosquito experiments for oocyst sample preparation . . . 24
4-3-5 TEM and serial block-face imaging by FIB-SEM . . . 25
4-4 Results
4-4-1 The 3D analysis of immature oocyst reconstruction of organelle architectures revealed endopolygeny-like nuclear segregation in *P. cynomolgi* . . . 25
4-4-2 The mature SPZ were observed inside oocysts with a divided nucleus accompanied by sophisticated organelle distribution . . . 27
4-5 Discussion . . . 28
4-6 Figures and movies legends . . . 30
4-7 Figures, movies and table . . . 34

Chapter 5.
General discussion 45

Acknowledgements 46
Reference 47

Abstract

The genus *Plasmodium* is a unicellular eukaryotic parasite that is the causative agent of malaria, which is transmitted by Anopheline mosquito. There are a total of three developmental stages in the production of haploid parasites in the *Plasmodium* life cycle: the oocyst stage in mosquitoes and the liver and blood stages in mammalian hosts. The *Plasmodium* oocyst stage plays an important role in the production of the first generation of haploid parasites. Nuclear division is the most important event that occurs during the proliferation of all eukaryotes. However, obtaining the details of nuclear division at the oocyst stage is challenging owing to difficulties in preparation. In this study, I used focused-ion-beam-milling combined with scanning-electron-microscopy to report the 3D architecture during nuclear segregations in oocyst stage. This advanced technology allowed us to analyse the 3D details of organelle segregation inside the oocyst during sporogony formation. It was revealed that multiple nuclei were involved with several centrosomes in one germ nucleus during sporozoite budding (endopolygeny). My high-resolution 3D analysis uncovered the endopolygeny-like nuclear architecture of *Plasmodium* in the definitive host. This nuclear segregation was different from that in the blood stage, and its similarity to other apicomplexan parasite nuclear divisions such as *Sarcocystis* is discussed.

Chapter 1. General Introduction

1-1 Malaria

Malaria is among the 3 major infectious diseases worldwide and is prevalent in tropical and subtropical regions. According to the WHO report in 2018, the number of malaria cases was 220 million and approximately 435,000 people died (Ghebreyesus & Admasu, 2018). Therefore, it is a major global health burden, which is difficult to eliminate because of the drug resistance of the parasite and the complexity of its life cycle. The protozoan parasites *Plasmodium* is the etiological agents of malaria that is transmitted by the Anopheline mosquito to human. The life cycle of *Plasmodium* development comprises of two proliferation stages in humans and one proliferation stage in Anopheline mosquito (oocyst stage). It is important to understand the mechanism of parasite proliferation especially nuclear segregation which is critical for parasite growth, in order to unveil not only the malaria biology but also for the next generation of anti-malaria (anti-protozoan disease) strategy. Multinuclear generation by closed mitosis occurs in all three proliferation stages of *Plasmodium* before dividing into daughter parasites, but the information regarding nuclear envelope division, especially multinuclear segregation within one parasite, remains limited.

1-2 Eukaryotic cell division

Eukaryotic cells have a tightly regulated proliferation with several variations of organelle segregation and are surrounded by a membrane structure. The cell nucleus is one of the most critical organelles in eukaryotes, and its multiplication is controlled by sophisticated mechanisms (Mitchison & Salmon, 2001; Scholey, Brust-Mascher, & Mogilner, 2003). The nucleus of the eukaryotic cell consists of chromosomes that are surrounded by a double-membrane nuclear envelope. During proliferation, nuclear division occurs and is accompanied either by nuclear envelope disassembly (open mitosis) or the maintenance of its intact structure before chromosome segregation (closed mitosis) (Boettcher & Barral, 2014). Open

mitosis has been observed in several eukaryotes such as mammalian cell, and chromosome segregation is accompanied by nuclear envelope disruption via several similar regulation mechanisms (Mitchison & Salmon, 2001; Scholey et al., 2003; Smoyer & Jaspersen, 2014). On the contrary, closed mitosis has been observed in unicellular organisms, such as protozoan parasites, and it is considered the most ancient mechanism of eukaryotic cell division (Cavalier-Smith, 2010). However, because the mechanisms of nuclear division during segregation in closed mitosis are highly divergent from each other, knowledge of the molecular machinery is limited, particularly on how nuclear envelope segregation is controlled during nuclear divisions in protozoan parasites (Aoki et al., 2011; Boettcher, Marquez-Lago, Bayer, Weiss, & Barral, 2012; Chang & Martin, 2009; Kubai & Ris, 1969; Perret, Davoust, Albert, Besseau, & Soyer-Gobillard, 1993; Shimoda, 2004; Yam, He, Zhang, Chiam, & Oliferenko, 2011).

1-3 Life cycle of the malaria parasite

Plasmodium is a genus of unicellular eukaryotic protozoan parasites that are the etiological agents of malaria, which is transmitted to mammalian hosts by the Anopheline mosquito. The life cycle of *Plasmodium* development comprises two proliferation stages in mammalians (liver and blood stages) and one proliferation stage in *Anopheles* (oocyst stage). Anopheline mosquitoes spread the infectious *Plasmodium* sporozoites (SPZs) by puncturing the human skin to feed on blood. Upon entering the bloodstream, the SPZs soon accumulate in the liver, where they invade hepatocytes to start liver stage development (White et al., 2014). Merozoite production occurs at the end of liver stage development, and the released merozoites invade red blood cells to cause symptomatic blood stage development by continually increasing in numbers. The proliferation during blood stage development involves closed mitosis, with the nuclear envelope maintaining its intact structure (Gerald, Mahajan, & Kumar, 2011; Mahajan et al., 2008; Roques et al., 2019). Nuclear division by closed mitosis occurs in all three

proliferation stages of *Plasmodium* species before dividing into daughter parasites. However, information regarding nuclear envelope division, particularly multinuclear segregation within one parasite, remains to be unveiled.

1-4 The electron microscopy analysis of the *Plasmodium*

The multinuclear segregation of blood stage parasites is called schizogony formation, which can be analysed in detail by using several types of light and electron microscopes. Blood stage development in closed mitosis has been observed using indirect immunofluorescence analysis and reveals nuclear division into two nuclei, similar to the process of closed mitosis in yeasts (Gerald et al., 2011; Mahajan et al., 2008; Roques et al., 2019). Several studies using transmission electron microscopy (TEM) and a limited number of studies using an advanced technology focused ion beam (FIB) milling combined with scanning electron microscopy (SEM) have clearly shown the structure of the divided parasites (Eshar, Dahan-Pasternak, Weiner, & Dzikowski, 2011; Medeiros, De Souza, Jiao, Barrabin, & Miranda, 2012; Sakaguchi, Miyazaki, Fujioka, Kaneko, & Murata, 2016; Weiner et al., 2011). It is difficult to show the processes in the middle of nuclear division (e.g., when the single nucleus divides into two nuclei) because the *Plasmodium* parasite is at its smallest size in the blood stage. Oocyst stage development has been observed using TEM or SEM, some of nuclei appeared in micrographs as irregular and elongate. Unfortunately, it was concluded that there were occasional invaginations of nuclear membrane due to the classical low resolution micrographs with only 2D analysis (Canning & Sinden, 1973; Howells & Davies, 1971).

1-5 The diversity of cell division in Apicomplexan parasites

The *Plasmodium* genus belongs to the phylum Apicomplexa, which includes genera *Toxoplasma*, *Cryptosporidium*, *Eimeria*, *Isospora* and *Sarcocystis*. The nuclear division of these apicomplexan parasites has been found to be extraordinarily divergent depending on

each parasite, and a possible change in the mechanism of nuclear division during each developmental stage has been reported for some of them (Ferguson, 2009; Ferguson et al., 2008; Francia & Striepen, 2014; Striepen, Jordan, Reiff, & van Dooren, 2007). It is known that the proliferation of *Sarcocystis neurona* occurs via endopolygeny, wherein multiple nuclei are divided from one germ nucleus (Vaishnava et al., 2005). On the contrary, endodyogeny has been observed in the proliferation of *Toxoplasma gondii*, in which two daughter cells are produced inside the mother cell with closed mitosis (Brooks et al., 2011; Nishi, Hu, Murray, & Roos, 2008; Suvorova, Francia, Striepen, & White, 2015). It was reported that the sexual developmental stage of *Toxoplasma* in the definitive host undergoes endopolygeny (Ferguson et al., 2007). Thus, variations in the mechanisms of nuclear division according to the parasite developmental stages are suggested in Apicomplexa.

In this study, I report detailed morphological differences in the oocyst stage development between *Plasmodium* species in the definitive host (Anopheline mosquito). Moreover, I present a 3D structural analysis of the nuclear divisions involved in endopolygeny-like segregation in oocyst stage development, in which multiple nuclei were connected with several centrosomes in one nucleus during the immature oocyst stage. Electron microscopy analysis revealed that *Plasmodium cynomolgi* (*Pcy*) oocyst stage development had a greater advantage in terms of cellular biology in the observation of organelle segregations. And also *Pcy* would be attractive target for future study due to have the dormant formation (called hypnozoite) in the liver stage development. The differences between the nuclear division mechanisms at the oocyst stage and schizogony at the blood stage are discussed.

Chapter 2. Morphological differences between malaria parasites in oocyst stage development by 2D-SEM

2-1 Abstract

Morphological differences of malarial parasites oocysts were observed by using a scanning electron microscopy (2D-SEM). These analysis clearly demonstrated that *P. cynomolgi* oocysts are larger than the rodent parasites oocysts, such as diameter, area and sporulation from the midgut.

2-2 Introduction

In older to compare the species specific morphological difference among *Plasmodium* oocysts in Anopheline mosquito, it is important use the same Anopheline species for several *Plasmodium* species. However, none of the reports has been used same Anopheline species to infect several variation of *Plasmodium* species. I expected to analyse the detail of morphological difference by electric microscopy, it is successfully to optimize the infectious condition of several *Plasmodium* species in *Anopheles stephensi*. I conducted SEM analysis of the rodent malarial parasites *P. berghei* (*Pb*) and *P. yoelii* (*Py*) and the primate malarial parasite *P. cynomolgi* (*Pcy*), each of which was infected with *A. stephensi*.

2-3 Materials and methods

2-3-1 Animal experiments and ethical committees

Two female Japanese macaques (5 years old; weighing 4.0－4.5 kg) were used for the experiment. The monkeys (*Macaca fuscata*) were provided by the National Bio Resource Project “Japanese macaques” at Kyoto University Primate Research Institute (Aichi, Japan). They were second-generation offspring bred in captivity, and they were bred and grown at animal facilities in a malaria-free environment in Japan. The infectious experiments for the monkeys were

performed under biosafety level 2 conditions at the Tsukuba Primate Research Center (TPRC), National Institute of Biomedical Innovation, Health and Nutrition, Ibaraki, Japan. The investigators adhered to the Guidelines for the Use of Experimental Animals authorised by the Japanese Association for Laboratory Animal Science. The protocol was approved by the Committee on the Ethics of Animal Experiments of the National Institute of Infectious Diseases Tokyo, Japan (for rodent experiments, permit number: 117108-II-2); Dokkyo Medical University, Tochigi, Japan (for primate experiments, permit number: 1007); and the TPRC (for primate experiments, permit number: DS29-14). The monkeys were used under the supervision of the veterinarians in charge of the animal facility.

2-3-2 Parasites and reporter parasites used

The *Plasmodium cynomolgi* B strain was obtained from ATCC (ATCC No. 30129) and maintained in Japanese macaques housed in the animal facility of Dokkyo Medical University, Japan. I used the rodent malaria parasites *Plasmodium berghei* and *Plasmodium yoelii*, which are the most common parasites utilised globally in experimental malaria models, transgenic *Pb*EF-GFP::Luc (676m1cl1) and *Py*GFP::Luc (1971). Information on the rodent parasite line can be found in the Rodent Malaria Genetically Modified Database (https://www.pberghei.eu/index.php).

2-3-3 Mosquito experiments for oocyst sample preparation

The laboratory-bred *Anopheles stephensi* mosquitoes were used for oocyst and sporozoite generation in this study. The colony of *An. stephensi* had been maintained in the Department of Parasitology, National Institute of Infectious Diseases (NIID), Japan (Tokyo, Japan). To develop oocysts in mosquitoes, *P. cynomolgi* B-infected blood was obtained from the donor monkey and fed into approximately 200 mosquitoes using the standard artificial membrane

feeding method (Annoura et al., 2014). The fed mosquitoes were kept in climate chambers at 24 °C with 80% humidity and fed regularly with 5% glucose-soaked cotton. The *Pcy*-infected mosquitoes were maintained in an incubator under BSL-3 condition at TPRC. Infection of mosquitoes with rodent parasites (*Pb* and *Py*) was done using canonical standard method under BSL2 condition at NIID (Annoura, Chevalley, Janse, Franke-Fayard, & Khan, 2013). Oocysts were obtained from dissected midgut at day 14-21 after blood-feeding. After collection, the midguts were fixed with 2.5% glutaraldehyde and 2% paraformaldehyde in 0.1 M phosphate buffer (pH 7.4) at 4 °C. The total number of mosquitoes required was dependent on the experiment and the number of oocysts per dissected mosquito.

2-3-4 Sample preparation for SEM

For SEM, the organs were fixed with 2% paraformaldehyde and 2.5% glutaraldehyde in 0.1 M phosphate buffer (pH 7.4) overnight at 4 °C, followed by postfixation with 1% OsO_4 in the same buffer. Thereafter, the fixed specimens were dehydrated in a graded series of ethanol. Then the ethanol was replaced with liquid CO_2 in the chamber of a critical point dryer (CPD 030; BAL-Tec), and the specimens were dried by critical point drying. After mounting on aluminium stubs with carbon paste, the dried specimens were coated with osmium by using a plasma coating device (Neoc-ST; Meiwafosis) and then observed with a scanning electron microscope (SU6600; Hitachi). The diameter of oocysts were measured using a measurement software (Quartz PCI 9; Quartz Imaging Corp).

2-4 Results

2-4-1 Morphological differences between rodent malaria parasites in oocyst stage development

Studies are lacking on the comparative analysis of the species-specific morphological differences in *Plasmodium* oocysts using the same Anopheline species (*Anopheles stephensi*). To observe the morphological differences in the *Plasmodium* oocyst stage, I employed two rodent malaria parasites, *P. berghei* (*Pb*) and *P. yoelii* (*Py*), for SEM analysis (Figs. 1A and 1B). The infected mosquito midguts and salivary glands (SGs) were collected under microscopy by hand dissection on several days from 14 to 21 days post-infection (dpi). To define the criteria for oocyst maturation, I counted the number of oocysts in the midgut and SPZs in the SG. Several hundred oocysts were observed under light microscopy with green fluorescent protein (GFP) positive in both *Pb* and *Py* (Figs. 1Aa–b and 1Ba–b), and fully mature oocysts were observed at 21 and 14 dpi for *Pb* and *Py*, respectively. These time points have previously been confirmed as the start of SPZ accumulation in the SG (Annoura et al., 2014). My SEM analysis clearly demonstrated the morphological differences between *Pb* and *Py* oocysts in both the diameter and thickness of the layer from the basal surface of the midgut. I employed the same *Anopheles stephensi* (*An. stephensi*) to set up the infection for *Pb* and *Py*, and most of the oocysts of both parasites were covered by the muscle tissue of the midgut (Figs. 1Ad–f and 1Bd–f). My observations revealed that the major difference between *Pb* and *Py* oocysts occurred in the distal portion of the protrusion from the midgut tissue (Table 1), wherein the *Py* oocysts bulged out more from the midgut than *Pb* oocysts. The surface of the *Pb* oocysts was observed as a smooth membrane structure (Figs. 1Ad and 1Ae), but some *Py* oocysts demonstrated a membrane structure with a thorny appearance (Figs. 1Bd and 1Be). The difference in the surface structure appeared to be species specific and was not associated with maturation because the number of *Py* oocysts with a thorny appearance did not increase. The mature parasites SPZs were observed by the start of budding and the initiation of the release

of SPZ from the oocysts (Figs. 1Ag and 1Bg).

2-4-2 The protruding oocyst with a smooth membrane appearance was connected to the mosquito basal membrane in *P. cynomolgi*

I succeeded in optimising the conditions for a high rate of infection for several *Plasmodium* species by using the same *An. stephensi*. I collected a large number of *P. cynomolgi* (*Pcy*)-infected *An. stephensi* midguts at 21 dpi (Fig. 2a) and fixed them for SEM analysis to observe the fully matured oocysts (Figs. 2b–j). Furthermore, basal-membrane-connected oocysts were frequently observed in *Pcy* (Figs. 2c, 2d and 2g. White arrowheads). Some of the fully matured *Pcy* oocysts with small cracked halls showed the ongoing budding out of SPZs inside the oocysts (Figs. 2h and 2i). I found that hundreds of SPZs were still connected to the midgut by a basal residual core body (Rb) (Figs. 2i and 2j), and this is known as sporogony formation. The size of the Rb shrunk when SPZs matured during budding (Figs. 2i and 2j). The sporogony form of parasites was observed in one oocyst, and these forms were separated and packed against each other. My SEM analysis of *Pcy* oocysts revealed that this was the best timing to observe the production of SPZs for the future investigation of organelle segregation.

2-4-3 Evaluation of oocyst diameter size and flat area in each *Plasmodium* parasite

The diameter and area of the *Pcy* oocysts were 17.4 ± 1.3 μm and 961 ± 143 μm^2, respectively (Table 1). These results clearly indicated that the *Pcy* oocysts were larger than the rodent parasites (Figs. 2b, 2e and 2f).

2-5 Discussion

These SEM analysis for oocysts were clearly indicated the morphological difference in several *Plasmodium* species. These results demonstrated that *Pcy* oocysts were larger than the rodent

parasites oocysts. It is suggested that *Pcy* oocysts produces large number of SPZ production, and suitable for further experiment such as a SPZ development and generation.

2-6 Figure Legends

Figure 1. Morphological differences of rodent malaria parasites in the oocyst stage of development

A. Fully mature *Pb*-oocyst development in the mosquito midgut at 21 dpi (*Pb*; 676m1cl1). **B.** Fully mature *Py*-oocyst development in the mosquito midgut at 14 dpi (*Py*; 1971). Visualisation of the infected mosquito midgut. **A, B.** (**a**) Bright-field microscopy. (**b**) GFP fluorescence signal (488 nm). (**c–g**) Observation of the infected mosquito midgut using SEM. (**g**) Newly hatched SPZs from oocysts were observed. White arrowheads, oocyst; Yellow line, midgut. The scale is shown in each image.

Figure 2. Observation of the oocyst in *Pcy*. Fully mature *Pcy*-oocyst development in mosquito midgut at 21 dpi. Visualisation of the infected mosquito midgut.

(**a**) Bright-field microscopy. (**b–j**) SEM. (**f–j**) High-magnification images of the oocyst. (**g**) Each hatched oocyst was connected by the muscle tissue of the mosquito. (**h–j**) Sporogony formation was observed inside mature oocysts. White arrowheads, basal-membrane-connected oocysts; Rb, residual core body. The scale is shown in each image.

Figure 1

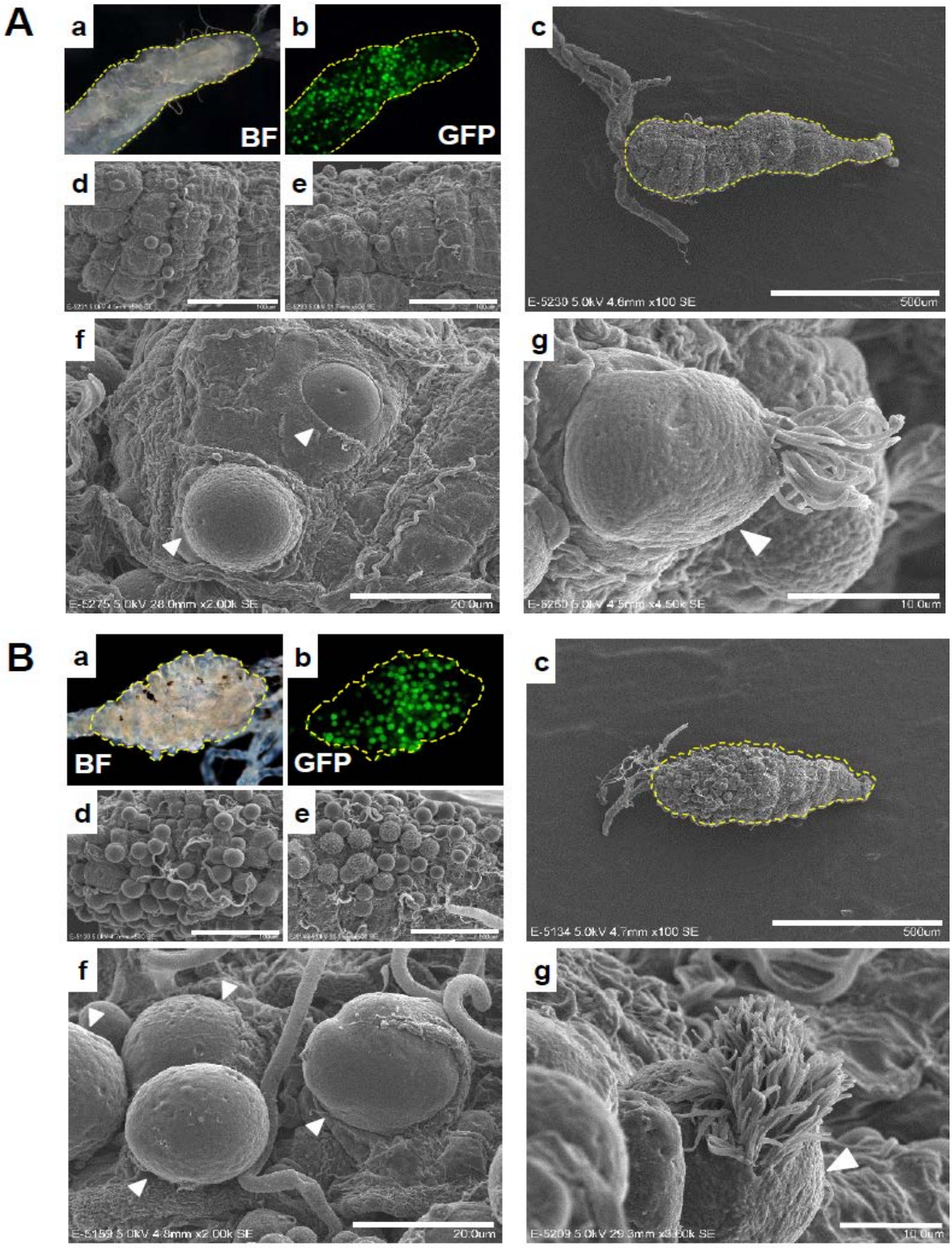
A
a
BF
b
GFP
c
d
e
E-5230 5.0kV 4.6mm x100 SE
500um
f
g
E-5275 5.0kV 28.0mm x2.00k SE
20.0um
10.0um
B
a
BF
b
GFP
c
d
e
E-5134 5.0kV 4.7mm x100 SE
500um
f
g
E-5159 5.0kV 4.8mm x2.00k SE
20.0um
10.0um

Figure 2

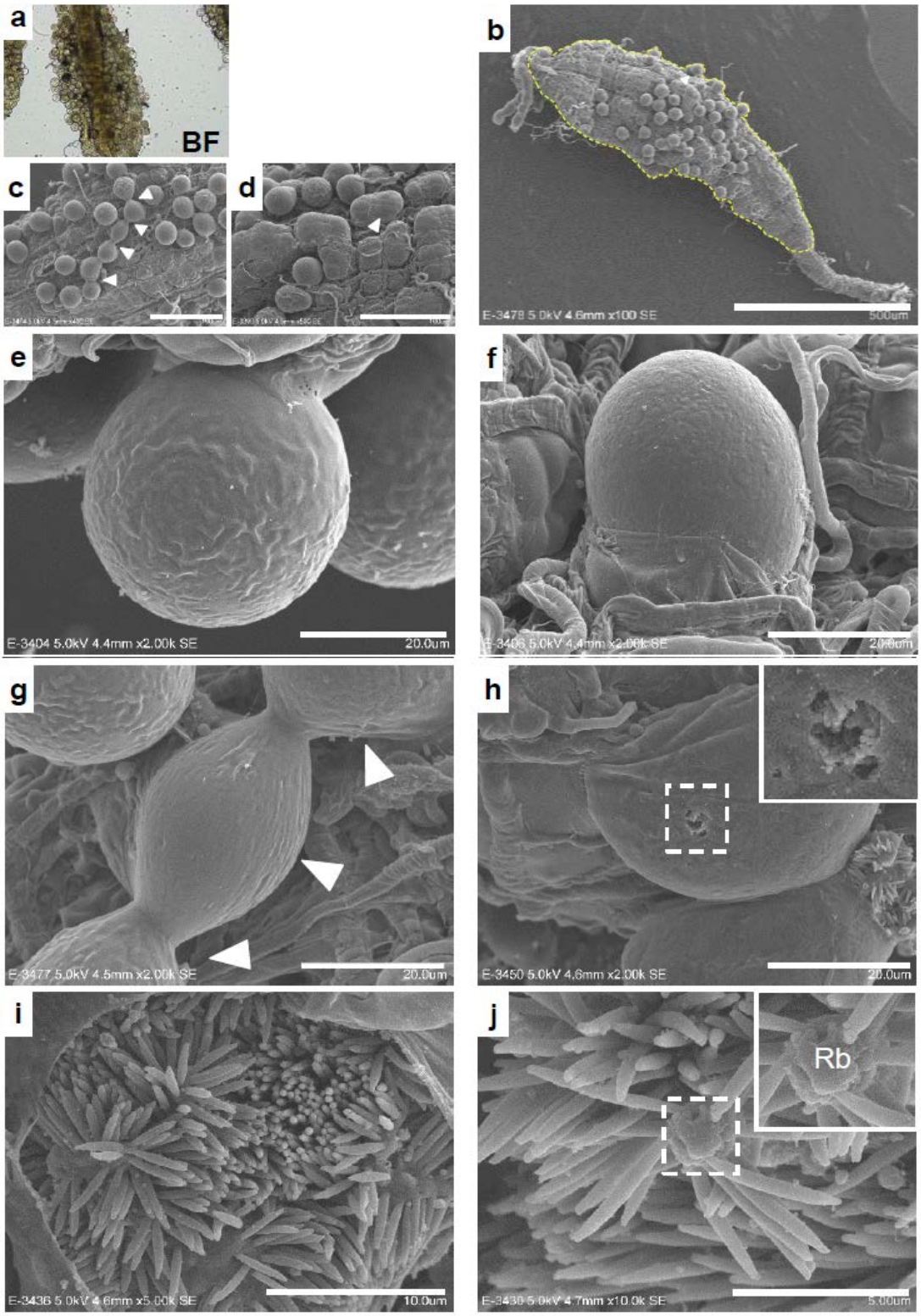
a
BF
b
E-3478 5.0kV 4.6mm x100 SE
500um
c
d
e
E-3404 5.0kV 4.4mm x2.00k SE
20.0um
f
g
E-3477 5.0kV 4.5mm x2.00k SE
20.0um
h
E-3450 5.0kV 4.6mm x2.00k SE
20.0um
i
E-3436 5.0kV 4.6mm x5.00k SE
10.0um
j
Rb
E-3430 5.0kV 4.7mm x10.0k SE
5.00um

Table 1

Evaluation of oocyst diameter size and flat area in each *Plasmodium* parasite. These oocysts used for the measurement were those just before midgut egression.

	Average ± SD	
Species	**Area (μm^2)**	**diameter (μm)**
P. berghei	207 ± 36	8.1 ± 0.7
P. yoelii	418 ± 103	11.4 ± 1.4
P. cynomolgi	961 ± 143	17.4 ± 1.3

Chapter 3. The 3D-structural reconstruction of sporozoites using classical array tomography

3-1 Abstract

In order to visualise the 3D structure of individual organelles architecture, I performed classical array tomography to observe the organelles of SPZ in serial-section images. However, my classical 3D-structure of mature SPZ was clearly shown artefacts, particularly organelles of SPZ with serious gaps. Moreover, the ability of the resolution for each organelles was insufficient for the further analyses, particularly organelle segregation.

3-2 Introduction

The mature SPZs are released from the oocyst, and accumulate to salivary gland (SG), which is the final platform for malaria parasites in the mosquito stage before infecting its mammalian host. In order to visualize the mature parasite organelles, the SG accumulated SPZ is one of the best options to observe the distribution of individual organelles. Accordingly, I performed classic array tomography to visualise this mature 3D SPZ structure with the architectures of individual organelles.

3-3 Materials and methods

3-3-1 Reporter parasites used

I used the rodent malaria parasites *Pb* and *Py*, which are the most common parasites utilised globally in experimental malaria models, transgenic *Pb*EF-GFP::Luc (676m1cl1) a. Information on the rodent parasite line can be found in the Rodent Malaria Genetically Modified Database. (https://www.pberghei.eu/index.php)

3-3-2 Mosquito experiments for SPZ sample preparation

The laboratory-bred *Anopheles stephensi* mosquitoes were used for sporozoite generation in this study. The colony of *An. stephensi* had been maintained in the Department of Parasitology, National Institute of Infectious Diseases (NIID), Japan (Tokyo, Japan). To develop SPZ in mosquitoes, *P. berghei* (*Pb*EF-GFP::Luc) infected blood was obtained from the donor ICR mice and fed into approximately 200 mosquitoes using the standard artificial membrane feeding method (Annoura et al., 2014). The fed mosquitoes were kept in climate chambers at 24 °C with 80% humidity and fed regularly with 5% glucose-soaked cotton. Infection of mosquitoes with *Pb* was done using canonical standard method under BSL2 condition at NIID (Annoura et al., 2013). SPZs were obtained from SGs on days 20–28. After collection, the midguts and SGs were fixed with 2.5% glutaraldehyde and 2% paraformaldehyde in 0.1 M phosphate buffer (pH 7.4) at 4 °C. The total number of mosquitoes required was dependent on the experiment and the number of SG SPZs per dissected mosquito.

3-3-3 TEM and classical 3D analysis

For TEM, the organs were fixed with 2% paraformaldehyde and 2.5% glutaraldehyde (TAAB Laboratories Equipment Ltd.) in 0.1 M phosphate buffer (pH 7.4) overnight at 4 °C, followed by postfixation with 2% OsO_4 in the same buffer. Thereafter, the fixed specimens were dehydrated with a graded series of ethanol and embedded in Epok 812 (Oken Shoji). Ultrathin sections were cut and stained with uranyl acetate and lead citrate and were then examined using an HT7700 transmission electron microscope (Hitachi). For the classical 3D analysis using an array tomography of the SPZs, the ultrathin serial sections of the SGs (70 nm thick) were cut, mounted on a glass coverslip and stained as described above. Thereafter, the sections were coated with osmium at a thickness of 2 nm by using an OPC80T osmium plasma coater (Filgen) and then observed using FIB-SEM on a Helios NanoLab 660. The 3D reconstruction was performed using Amira software (FEI).

3-4 Results

3-4-1 the majority of *Pb*-SPZ accumulation was observed in the epithelial cells of SG lateral lobes.

After the mature SPZs are released from oocyst, they accumulate in the SG, which is the final platform for malaria parasites in the mosquito stage before infection into a mammalian host. I employed transgenic GFP-expressing *Pb* to visualise SPZ accumulation in the SG lobes, and a strong GFP signal was detected only in the lateral lobes in *Pb*-infected *An. stephensi* at 21 dpi (Figs. 3Aa and 3Ab). I performed SEM analysis of the SGs to observe in detail the morphological differences between each lobe, and intumescence and swelling of the lateral lobes were clearly observed (Figs. 3Ba and 3Bb). Moreover, some of the lateral lobes contained SPZ (Fig. 3Bc) and numerous SPZs on their surfaces (Fig. 3Bd). To elucidate the details of SPZ accumulation in the SG, I performed classical array tomography of the *Pb*-infected SG lobes and found the typical morphology of SPZ accumulation in the lateral lobes. Moreover, the majority of SPZ accumulation was observed in the area of the epithelial cells, and very few SPZs were found in the secretory cavity and duct area (Figs. 4a and 4b).

3-4-2 Rodent malaria parasites in the SG, the quality of organelle resolution was insufficient by classical 3D structure analysis

To visualise the 3D structure of SPZ accumulation with the architecture of individual organelles, I performed classical array tomography (Fig. 3Cb). I successfully utilised this analysis to determine the 3D structure of the SPZ parasite (Fig. 3Ca) with 70 nm slice staining; however, my classical 3D structure for SPZ was clearly shown artefacts especially nuclear and apical end of SPZ with serious gap (Fig. 3Cb. White arrow), the quality of organelle resolution was insufficient for performing further analyses, particularly the analysis of organelle segregation and localisation.

3-5 Discussion

It was clearly observed the intumescence and swelling of *Pb*-infected lateral lobes by using SEM analysis. Moreover, numerous number of SPZs were founded on the surface of lateral lobes only. This classical 3D-structure analysis of SG-SPZ clearly shown artefacts, particularly those associated with the nucleus and plasma membrane of SPZ with serious gaps. Moreover, the resolution of organelles was insufficient for further analyses, particularly organelle segregation. Therefore, I used focused ion beam milling combined with scanning electron microscopy (FIB-SEM) analysis for the future experiments, which is the advanced the method for 3D analysis of an organelle. On the other hands, it was observed SPZs accumulation in middle lobe by another *Plasmodium* species (unpublished data). Further experiments are required to clarify for these interesting findings.

3-6 Figure Legends

Figure 3. Observation of SPZs in mosquito SG.

A. Visualisation of the *Pb* (*Pb;* 676m1cl1)–infected mosquito SG. (**a**) Bright-field microscopy. (**b**) GFP fluorescence signal (488 nm). **B.** (**a, b**) *Pb*-infected SG showing enlarged lateral lobes. (**c**) High-magnification of 2Ba. (**d**) High-magnification image of 2Bb. **C.** Serial ultrathin sections (70 nm thick) of the infected SG for classical 3D analysis. (**a**) A slice image. (**b**) Reconstructed 3D images of SPZ. White arrows, serious gaps by artefacts; Yellow line, SPZ plasma membrane; N (purple), nucleus; Rh (green), rhoptry. The scale is shown in each image.

Figure 4. The SPZ accumulation was observed in the area of epithelial cells.

Detailed observation of the SGs of infected mosquitoes using TEM. (**a**) SPZs were found in the epithelial cells and very few in the secretory cavity (Sc). (**b**) Schematic diagram of SG SPZs in SG epithelial cells. Yellow, SPZs.

Figure 3

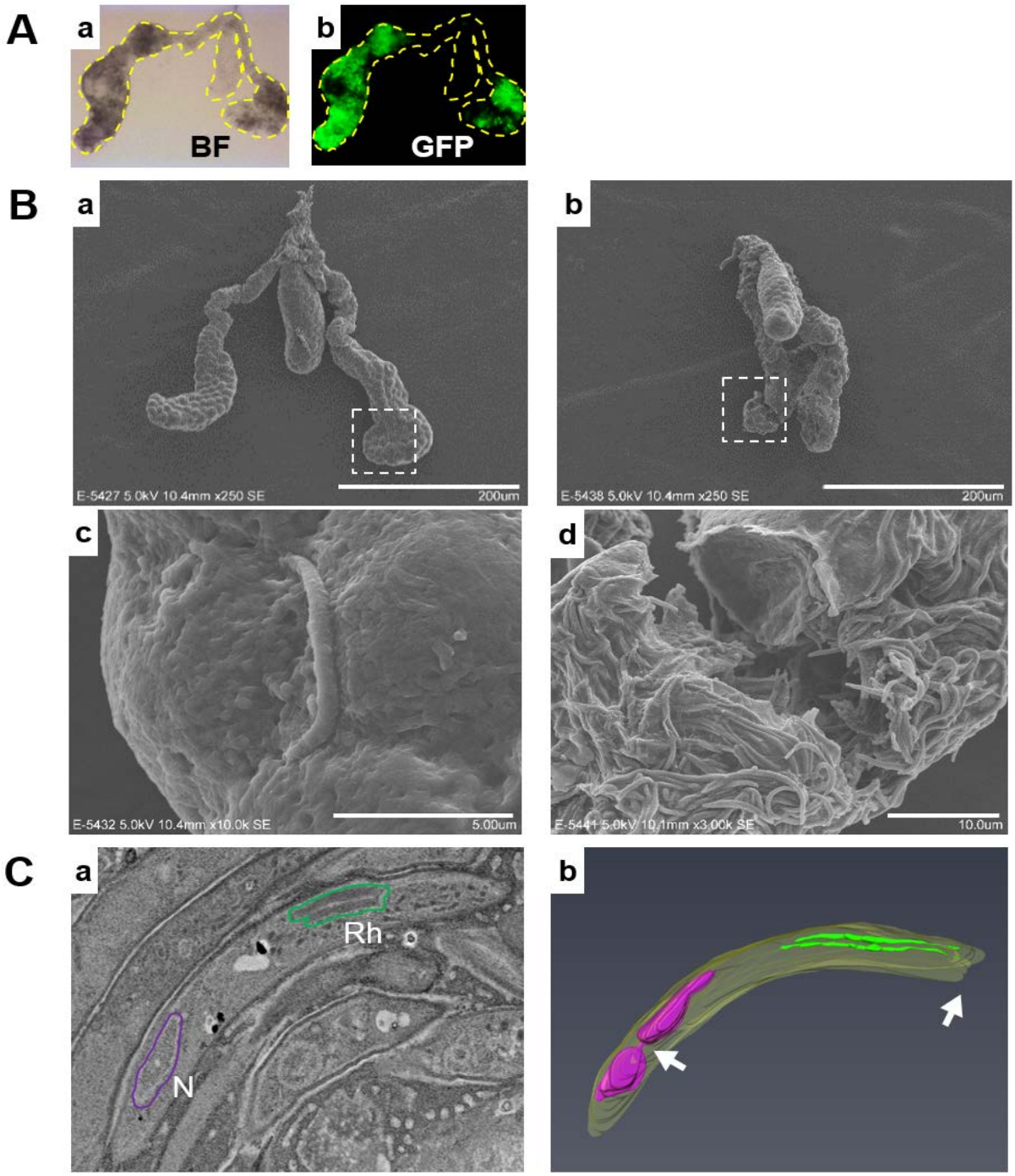
A
a
BF
b
GFP
B
a
E-5427 5.0kV 10.4mm x250 SE
200um
b
E-5438 5.0kV 10.4mm x250 SE
200um
c
E-5432 5.0kV 10.4mm x10.0k SE
5.00um
d
E-5441 5.0kV 10.1mm x3.00k SE
10.0um
C
a
Rh
N
b

Figure 4

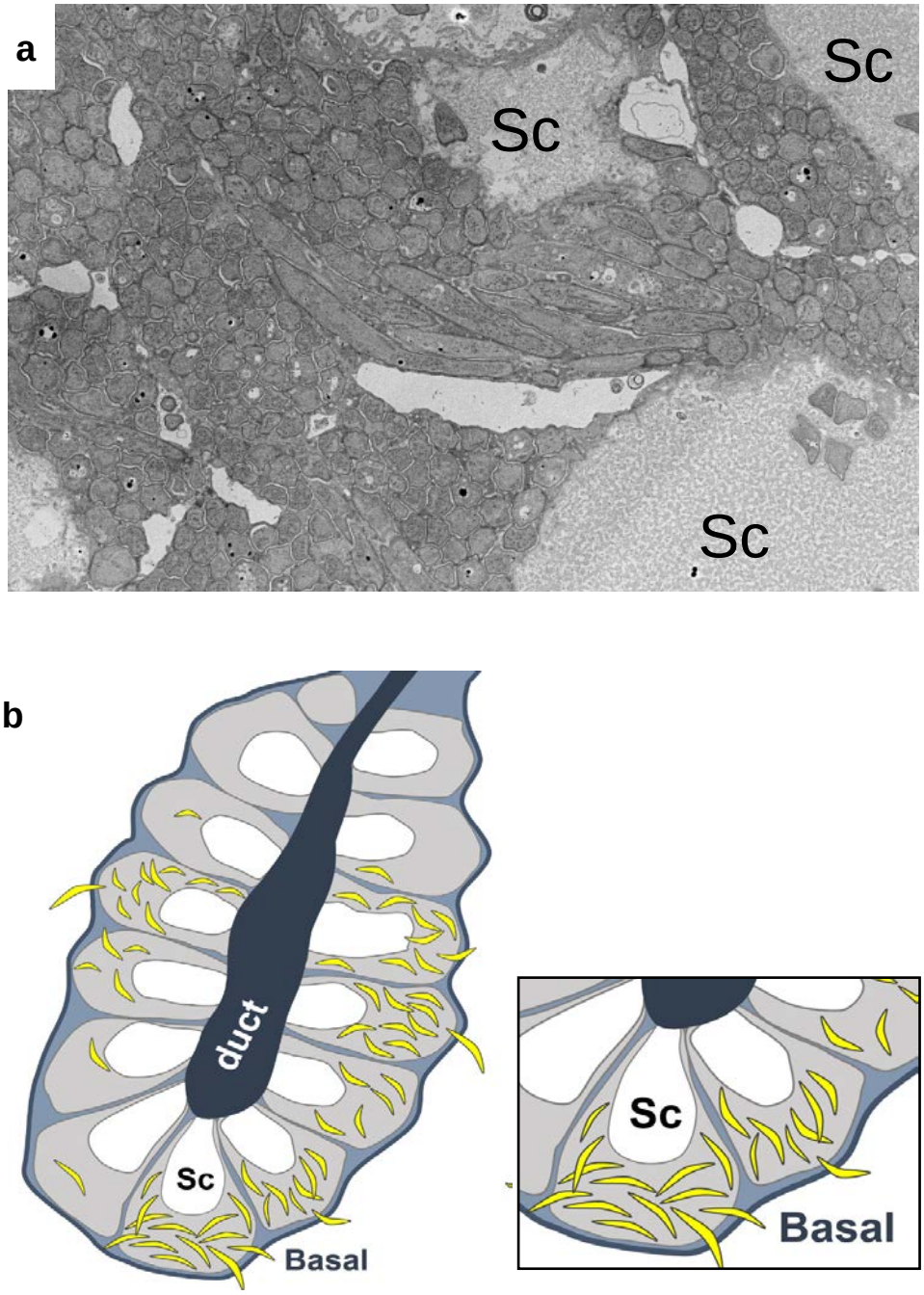

Chapter 4. Three-dimensional FIB-SEM analysis of the organelle segregation in *Plasmodium* oocyst development

4-1 Abstract

Nuclear division is the most important event that occurs during the proliferation for all eukaryotes. However, obtaining the details of nuclear division at the oocyst stage is challenging owing to difficulties in preparation. In this study, I used focused-ion-beam-milling combined with scanning-electron-microscopy (FIB-SEM) to observe the 3D architecture during nuclear segregations in oocyst stage. This advanced technology allowed us to analyse the details of organelle segregation inside the oocyst during sporogony formation. It was revealed that multiple nuclei were connected with several centrosomes in one nucleus during sporozoite budding (endopolygeny). My high-resolution 3D analysis uncovered the endopolygeny-like nuclear architecture of *Plasmodium* in the definitive host.

4-2 Introduction

The focused-ion-beam milling combination with FIB-SEM, which is the advanced electric microscopy suitable to analyse the detail of organelle segregation inside the cell (Kremer et al., 2015). I employed FIB-SEM to visualize the detail of organelle segregation, especially multinuclear segregation within one parasite. It has not been reported that the mechanism of nuclear division in oocyst stage. In older to observe the detail of nuclear segregation, I selected *Pcy* oocyst which is the largest oocyst and suitable for my further experiments. Here I conducted the 3D-analysis of nuclear architecture segregation in oocyst stage development, which revealed the endopolygeny-like nuclear division are occurred in *Plasmodium*.

4-3 Materials and methods

4-3-1 Animal experiments and ethical committees

Two female Japanese macaques (5 years old; weighing 4.0－4.5 kg) were used for the experiment. The monkeys (*Macaca fuscata*) were provided by the National Bio Resource Project "Japanese macaques" at Kyoto University Primate Research Institute (Aichi, Japan). They were second-generation offspring bred in captivity, and they were bred and grown at animal facilities in a malaria-free environment in Japan. The infectious experiments for the monkeys were performed under biosafety level 2 conditions at the Tsukuba Primate Research Center (TPRC), National Institute of Biomedical Innovation, Health and Nutrition, Ibaraki, Japan. The investigators adhered to the Guidelines for the Use of Experimental Animals authorised by the Japanese Association for Laboratory Animal Science. The protocol was approved by the Committee on the Ethics of Animal Experiments of the National Institute of Infectious Diseases Tokyo, Japan (for rodent experiments, permit number: 117108-II-2); Dokkyo Medical University, Tochigi, Japan (for primate experiments, permit number: 1007); and the TPRC (for primate experiments, permit number: DS29-14). The monkeys were used under the supervision of the veterinarians in charge of the animal facility.

4-3-2 Parasites and reporter parasite used

The *P. cynomolgi* B strain was obtained from ATCC (ATCC No. 30129) and maintained in Japanese macaques housed in the animal facility of Dokkyo Medical University, Japan. I used the rodent malaria parasite *Plasmodium berghei*, which parasite is overexpress *sas6-mCherry*; *Pb*SAS6-$_{mChcon}$ (for more information 4-3-2).

4-3-3 Generation of transgenic *Pb* line *Pb*SAS6-$_{mChcon}$

*Pb*SAS6-$_{mChcon}$ is a transgenic *Pb* line that overexpresses the fusion protein *Pb*SAS6–mCherry from the *hsp70* promoter and is drug-selectable marker (SM) free. The construct UMV1-*Pb*SAS6 was made for the generation of transgenic lines that expressed *Pb*SAS6 and mCherry reporter under the *hsp70* promoter. The construct used to target the GIMO$_{pbANKA}$ line was made using the gene insertion/marker out method; therefore, it did not contain any drug-SM (Lin et al., 2011). The UMV1-*Pb*SAS6 construct was generated by cloning the 5' and 3' ends of *Pb*SAS6, which were amplified from *Pb* genomic DNA by using polymerase chain reaction (PCR) assays (see Supplementary Table 1 for the primer sequences), into UMV1 (containing both 5' *hsp70* and 3' *hsp70* sequences, *mCherry* cassette and *230p* targeting regions) upstream of the *mCherry* cassette by using a *Bam*HI restriction site. Therefore, the UMV1-*Pb*SAS6 constructs possessed the 5' *hsp70–Pbsas6–mCherry*-3' *hsp70* expression cassette and 230p targeting sequences and no SM. The constructs were linearised by SacII digestion prior to transfection. Transfection was performed using the schizonts of the GIMO$_{pbANKA}$ line. The selection of transformed and transgenic parasites was performed using negative selection with 5-FC as previously described (Lin et al., 2011), thus resulting in the generation of *Pb*SAS6-mChcon parasites. Super-resolution imaging was undertaken using a spinning disk super - resolution microscope (SpinSR10; Olympus, Tokyo, Japan) with UPLSAPO60XS2 oil immersion objective lens (Olympus). Fluorescence images were processed using ImageJ software (Bethesda, MD, USA).

4-3-4 Mosquito experiments for oocyst sample preparation

The laboratory-bred *Anopheles stephensi* mosquitoes were used for oocyst and sporozoite generation in this study. The colony of *An. stephensi* had been maintained in the Department of Parasitology, National Institute of Infectious Diseases (NIID), Japan (Tokyo, Japan). To develop oocysts in mosquitoes, *P. cynomolgi* B-infected blood was obtained from the donor

monkey and fed into approximately 200 mosquitoes using the standard artificial membrane feeding method (Annoura et al., 2014). The fed mosquitoes were kept in climate chambers at 24 °C with 80% humidity and fed regularly with 5% glucose-soaked cotton. The *Pcy*-infected mosquitoes were maintained in an incubator under BSL-3 condition at TPRC. Oocysts were obtained from dissected midgut at day 14-21 after blood-feeding. After collection, the midguts were fixed with 2.5% glutaraldehyde and 2% paraformaldehyde in 0.1 M phosphate buffer (pH 7.4) at 4 °C. The total number of mosquitoes required was dependent on the experiment and the number of oocysts per dissected mosquito.

4-3-5 TEM and serial block-face imaging by FIB-SEM

For TEM, the organs were fixed with 2% paraformaldehyde and 2.5% glutaraldehyde (TAAB Laboratories Equipment Ltd.) in 0.1 M phosphate buffer (pH 7.4) overnight at 4 °C, followed by postfixation with 2% OsO_4 in the same buffer. Thereafter, the fixed specimens were dehydrated with a graded series of ethanol and embedded in Epok 812 (Oken Shoji). Ultrathin sections were cut and stained with uranyl acetate and lead citrate and were then examined using an HT7700 transmission electron microscope (Hitachi). For the serial block-face SEM of oocysts, images were taken using FIB-SEM on a Helios NanoLab 660 (FEI). The Epon blocks of midguts were milled using a FIB, and the serial block-face imaging of the oocysts was performed every 40 nm by using a backscattered electron detector (MD detector) at an acceleration voltage of 2.0 kV and a current of 0.4 nA.

4-4 Results

4-4-1 The 3D analysis of immature oocyst reconstruction of organelle architectures revealed endopolygeny-like nuclear segregation in *P. cynomolgi*

Multinuclear segregation has been well studied in blood stage parasites, wherein the parent nucleus divides into two daughter nuclei without the segregation of the plasma membrane of

the parasite. This is known as schizogony development (Francia & Striepen, 2014; Gerald et al., 2011). To observe the details of nuclear segregation at the oocyst stage so that the differences from schizont segregation could be determined, I analysed *Pcy*-infected midguts, which is the largest and longest period to generate SPZ productions, by using FIB-SEM. This is one of the best options for the monitoring of nuclear division. *Pcy*-infected midgut was dissected at 14 dpi, which was expected to be the middle of the proliferation period and is when the most drastic changes of organelle segregation occur. The images of semithin section slides with toluidine blue staining clearly showed the oocyst morphology (Fig. 5Aa. Black square), and this was confirmed by TEM analysis as sporogony formation (Figs. 5Ab and 5Ac). It was easy to recognise the apical ends of the SPZs because of the high electron-dense of plasma membrane and rhoptries (high-electron-dense organelle). These observations clearly indicated that the state of these oocysts was still immature because the SPZ plasma membrane (Fig. 5Ac. Black line) was still bonded, and many rhoptries were located in the same budding SPZ (Figs. 5Ab and 5Ac). To reveal the details of organelle segregation in SPZs production, I performed FIB-SEM analysis by using the immature oocyst. My analysis showed that most of the immature SPZ contained several rhoptries (Figs. 5Ac, 5Ba and 5Ca. Green arrowheads) that are located near the apical end of the plasma membrane. The apical ends of the SPZs were not yet well protruded because the budding parasites are still incomplete, and I could also observe Rbs in the centre of the sporogony formation of these immature parasites (Fig. 5Ac). To clarify the nuclear segregation of immature oocyst, I conducted a 3D analysis of these parasites. I obtained approximately 200–500 serial block-face of images/oocyst, and sporogony formation parasites that contained rhoptries and the whole nucleus within a series of slices were selected for 3D analysis. The nuclei of these parasites were also found to be centrosome positive, as evidenced by a high electron-dense with a typical centrosome shape on the edge of the nuclear envelope. A series of slides revealed that these centrosomes were located on the same nucleus (Figs. 5Ba slices 130 and 132. Orange arrowheads). The

segmentation of each organelle for 3D analysis was performed by colour staining. Figures 4Bb and 4Cb shows the 3D reconstructed images and videos (Movies. 1 and 2). These videos clearly indicated that the nuclear envelope of immature oocyst was bonded with multiple centrosome-positive nuclei (Movie 1), and this process is similar to endopolygeny. Moreover, in the simple and clear examples of multiple centrosome-positive nuclear images that I obtained (Figs. 5Ca, 5Cb and Movie 2), nuclear division showed an endopolygeny-like structure that was unmistakably different from that of schizonts. This was the first demonstration of *Plasmodium* endopolygeny-like nuclear architecture in the definitive host.

4-4-2 The mature SPZ were observed inside oocysts with a divided nucleus accompanied by sophisticated organelle distribution

My 3D-electron microscopy analysis of immature oocyst nuclear architecture revealed that endopolygeny-like segregation occurred in *Plasmodium cynomolgi* in the definitive host for this parasite. To follow up on this unique nuclear segregation, I performed the same analysis at a later time point of oocyst stage development. At 21 dpi, *Pcy*-infected *Anopheles* midguts were dissected to observe the morphological differences of parasite development regarding organelle segregation and distribution, particularly the nuclear architecture. My TEM analysis (Fig. 6A) revealed that the SPZ plasma membrane structures were well partitioned into the divided SPZs, with several intact mature organelles, such as rhoptries. Furthermore, large size of Rb was difficult to find at this time point. These observations indicated that the fully mature and final stage of oocyst development to produce the SPZs occurred at 21 dpi. The FIB-SEM analyses of several *Pcy*-infected mosquito midguts were performed using serial sections of 150 images per 40 nm, and Figure 5B presents the typical images. Enlarged and well-parcellated mature rhoptries were observed inside SPZs as highly electron-dense organelles (Fig. 6Ba. Green arrowhead) accompanied by distributed nuclei. Alternative or immature organelles are distinguishable from mature rhoptry (AOR), which are clearly different from

mature rhoptries because of a different electron-dense and are surrounded by a double membrane, were observed between the rhoptries and the nucleus (Fig. 6Bb. Blue arrowhead). AOR was not observed in the immature oocyst at 14 dpi. The elongated parasite nucleus was well partitioned and divided into each nucleus one by one for SPZ generation. The 3D reconstructed structure images (Figs. 6Ca and 6Cb) clearly showed the organelle distributions of the divided SPZs and demonstrated the orchestrated ordered assembly for each organelle (Rhoptries, AORs and nucleus) (Fig. 6C, Movies 3 and 4). The centrosome structures were not observed in well-partitioned parasite nuclei at this time point. Centrosomes are essential only for chromosome distribution and segregation; therefore, these results indicated that the parasite had already completed these nuclear segregation processes.

The schematic diagrams of nuclear division in *Plasmodium* and *Sarcocystis neurona* were shown in Figure 7. It has been reported in *Plasmodium* that schizogony formation was observed as multinuclear segregation in blood stage parasites. In the schizont stage, the mother nucleus divides into two daughter nuclei, and this process of multiple nuclear fission was continually repeated (Gerald et al., 2011; Mahajan et al., 2008; Roques et al., 2019). The current study is the first report of endopolygeny-like proliferation in *Plasmodium* oocyst stage development with the mother nucleus divided into more than three nuclei at the same time, which is similar to the *Sarcocystis* nuclear division (Vaishnava et al., 2005).

4-5 Discussion

In this study, I revealed the occurrence of endopolygeny-like nuclear architecture segregation in *Plasmodium* oocyst development. This was similar to the nuclear segregation reported in another protozoan parasites, such as a *Sarcocystis neurona*. My 3D FIB-SEM analysis clearly showed that the immature oocyst mother nucleus was divided into several daughter nuclei that were joined by a network formation. Analysis using 3D FIB-SEM is advantageous because it can resolve organelle structure, particularly the high resolution of the membrane architecture

of each organelle, in far greater detail than other techniques. There are a limited number of articles that detail the 3D architecture of organelles by FIB-SEM for the *Plasmodium* blood stage because of the small size of the parasite (Eshar et al., 2011; Medeiros et al., 2012; Sakaguchi et al., 2016; Weiner et al., 2011). These FIB-SEM studies have mainly focused on the architecture of parasite-specific organelles in the blood stage, and none of them reported on the other developmental stages.

I need to ask why the endopolygeny-like formation in *Plasmodium* was not previously discovered. Some of classical EM articles had been mentioned occasional invaginations of nuclear membrane with irregular and elongate shape in oocyst stage development. However, it was difficult to observe endopolygeny-like structure by using the classical EM analysis in *Plasmodium* (Canning & Sinden, 1973; Howells & Davies, 1971). Although advanced 3D FIB-SEM analysis has made it possible to obtain the high-resolution images of nuclear architecture, this was previously difficult to obtain using classical array tomography 3D analysis. Another possibility is that the confocal microscopy images using Hoechst or 4′,6-diamidino-2-phenylindole DNA staining in the oocyst stage could have been misleading. These DNA staining methods bind with a high affinity to the minor groove of AT-rich DNA sequences. It has been reported in several articles that Hoechst signals with dots were shown in nuclei in the late oocyst stage of development. However, these signals did not show all the nuclear areas, particularly during nuclear division, because the signals became weak or disappeared when the DNA became relaxed. To visualise the nuclear segregation, I generated a reporter parasite line with SAS6 (spindle assembly abnormal protein 6 homolog) c-terminal tagging by mCherry in *Pb*. SAS6 is one of the best markers for centrosomes and is recruited to centrioles at the onset of the centrosome duplication cycle (Suvorova et al., 2015). Although strong SAS6–mCherry signals were detected in the oocyst stage, most oocysts with a strong SAS6–mCherry signal showed an undetectable level of Hoechst signal. On the other hand, oocysts with a strong Hoechst signal showed an undetectable level of SAS6–mCherry signal (Fig. 8C). It is

suggested that SAS6–mCherry-positive oocysts were undergoing nuclear division and that SAS6–mCherry-negative oocysts had completed nuclear division. These unexpected results led us to the realisation that the shape of the oocyst nucleus might not be reflected by the Hoechst signal (Fig. 8C), and future experiments are necessary to clarify these possibilities. My 3D FIB-SEM analysis revealed not only the endopolygeny-like nucleus in the oocyst stage of development but also the appearance of AORs. Owing to the difference in electron density, differentiating AORs from rhoptries was easily performed. Several additional experiments are required to determine the nature of specific organelles, and it is possible that AORs could be immature rhoptry, pro-micronemes, immature dense granules or other unknown organelles (Schrevel et al., 2008). The 3D FIB-SEM analysis of the oocysts of rodent malaria parasites on several different post-infection days could provide more information.

4-6 Figures and movies legends

Figure 5. Immature *Pcy*-oocyst development in mosquito midgut at 14 dpi.

A. (**a**) *Pcy*-infected oocyst semi-thin sections were stained with toluidine blue. (**b, c**) Visualisation of the sporulating SPZs in oocyst from the serial section images using TEM. Rb, residual core body; green arrowheads, rhoptry. **B, C**. (**a**) Serial images of individual budding SPZ show three centrosomes. Orange arrowhead, centrosome; Green arrowheads, Rhoptry; N, nucleus. (**b**) Reconstructed 3D images of immature sporogony formation. Purple, nucleus; orange, centrosome; yellow, SPZ inner membrane; green, rhoptry. See also **Movie 1** of Fig. 5Bb and **Movie 2** of Fig. 5Cb.

Figure 6. Three-dimensional analysis of the organelle of mature *Pcy* oocysts using FIB-SEM. At 21dpi, the nucleus was divided, and the other organelles were more developed.

A. Visualisation of the sporulating SPZs in oocysts from the serial section images using TEM. **B.** Observation of the mature SPZ formation in oocysts from the serial block-face images. (**a**) The green arrowhead indicates developing rhoptry. (**b**) The blue arrowhead indicates AOR. **C.** Reconstructed partial 3D images of mature sporogony formation. Purple, nucleus; yellow, SPZ inner membrane; green, rhoptry; blue, AOR. See also **Movies 3** and **4** of Fig. 6C.

Figure 7. Schematic diagrams of the nuclear division in *Plasmodium*, *Sarcocystis and Toxoplasma*: *Plasmodium* (schizogony [blood stage] and endopolygeny-like [oocyst stage]), *Sarcocystis* (endopolygeny), Toxoplasma (endodyogeny and endopolygeny).

Purple, nucleus; orange, centrosome; yellow, SPZ inner membrane; green, rhoptry; blue, AOR; white arrow, direction of nuclear division.

Figure 8. Generation of transgenic *Pb*SAS6-mC$_{hcon}$ expressing *mCherry* under the control of the *hsp70* promoter.

A. Schematic representation of the *Pb*SAS6–mCherry expression cassettes into GIMO$_{pbANKA}$. Construct UMV1-*Pb*SAS6 contains the *hsp70* promoter (5' *hsp70*)–*Pb*SAS6–mCherry-3' *hsp70* cassette. This DNA construct is integrated into the modified *Pb 230p* locus containing the *hdhfr*::*yfcu* SM cassette by double cross-over homologous recombination at the target regions (grey boxes). Negative selection with 5-FC selects for the transgenic parasite line *Pb*SAS6-mC$_{hcon}$ that has the 5' *hsp70–Pb*SAS6–mCherry-3*' hsp70* expression cassettes introduced into the *230p* locus due to remove the *hdhfr*::*yfcu* negative selection marker. The location of primers used for PCR analysis (see **B**) and the sizes of the PCR products are shown (see Table 2 for primer sequences). **B.** Diagnostic PCR analysis confirms the correct integration of construct UMV1-*Pb*SAS6 in line *Pb*SAS6-mC$_{hcon}$, as shown by the absence of the *hdhfr*::y*fcu* marker and the presence of the *mCherry* gene: 5' integration PCR (5'; primers

5510 and J0561), 3' integration PCR (3'; primers J0477 and 5511), amplification of SAS6–*mCherry* (sas6-mC; primers J0539 and J0480) and SM (SM; primers 5510 and 4699). The primer locations and product sizes are shown in **A** (see Table 2 for primer sequences).**C.** Fluorescence microscopy of *Plasmodium* oocyst from a mosquito at day 21 after infection (see also Movies 5 and 6).

Movie 1. The 3D reconstructed structural images in immature oocysts at 14 dpi (Fig. 5Bb movie).

Purple, nucleus; orange, centrosome; yellow, SPZ inner membrane; green, rhoptry.

Movie 2. The 3D reconstructed structural images in immature oocysts at 14 dpi (Fig. 5Cb movie).

Purple, nucleus; orange, centrosome; yellow, SPZ inner membrane; green, rhoptry.

Movie 3. The 3D reconstructed structural images in mature oocyst for SPZ generation at 21 dpi (Fig. 6Ca movie).

Purple, nucleus; yellow, SPZ inner membrane; green, rhoptry; blue, AOR.

Movie 4. The 3D reconstructed structural images in mature oocyst for SPZ generation at 21 dpi (Fig. 6Cb movie).

Purple, nucleus; yellow, SPZ inner membrane; green, rhoptry; blue, AOR.

Movie 5. Fluorescence microscopy of *Plasmodium* oocyst from a mosquito at day 21 after infection (Fig. 8C movie).

The oocyst was observed with strong mCherry signals in *Pb*SAS6-mC_{hcon}.

Movie 6. Fluorescence microscopy of *Plasmodium* oocyst from a mosquito at day 21 after infection (Fig. 8C movie).

The oocyst was observed with low mCherry signals in *Pb*SAS6-mC_{hcon}.

Figure 5

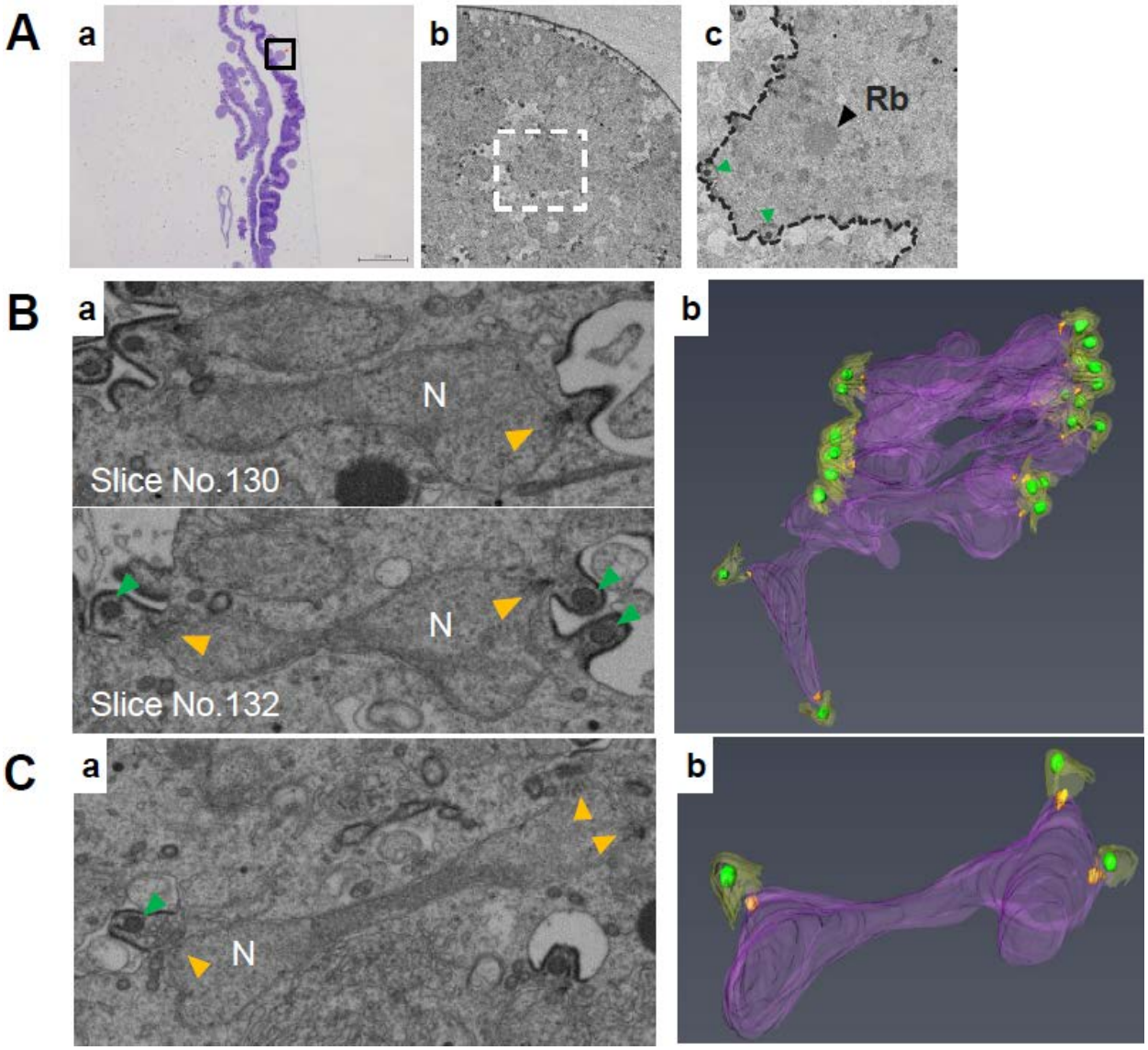

Figure 6

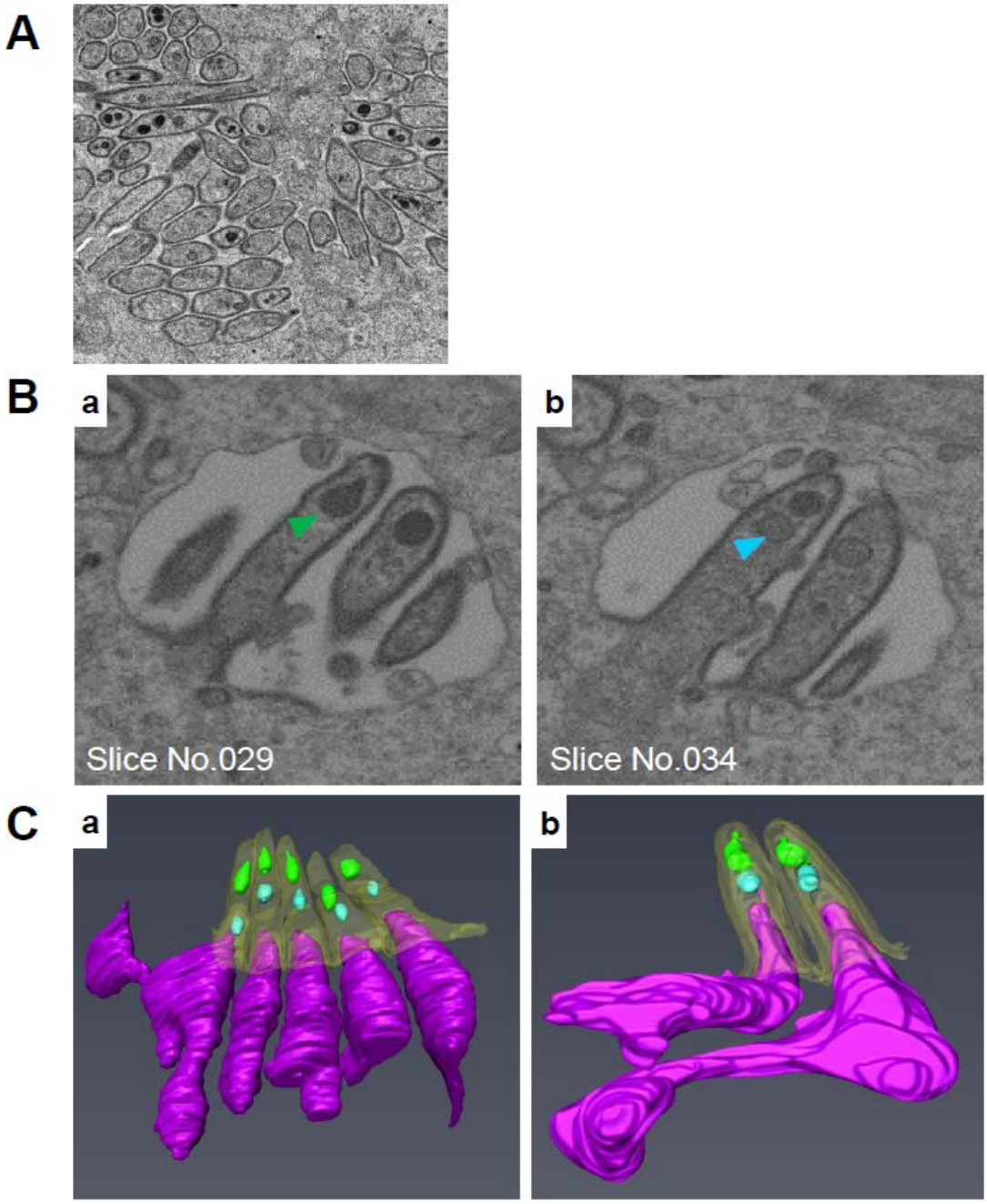

Figure 7

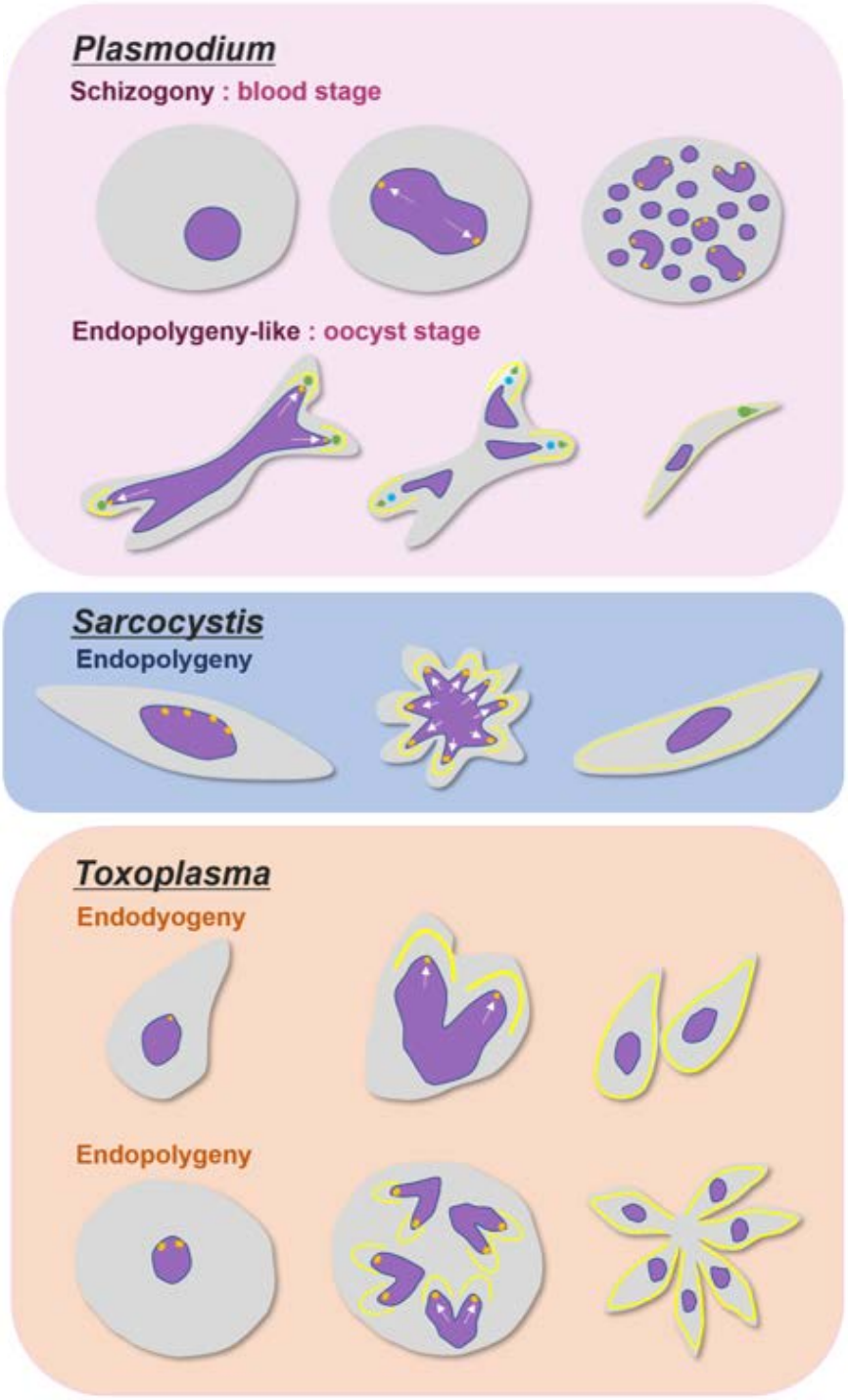
Plasmodium
Schizogony : blood stage
Endopolygeny-like : oocyst stage
Sarcocystis
Endopolygeny
Toxoplasma
Endodyogeny
Endopolygeny

Figure 8

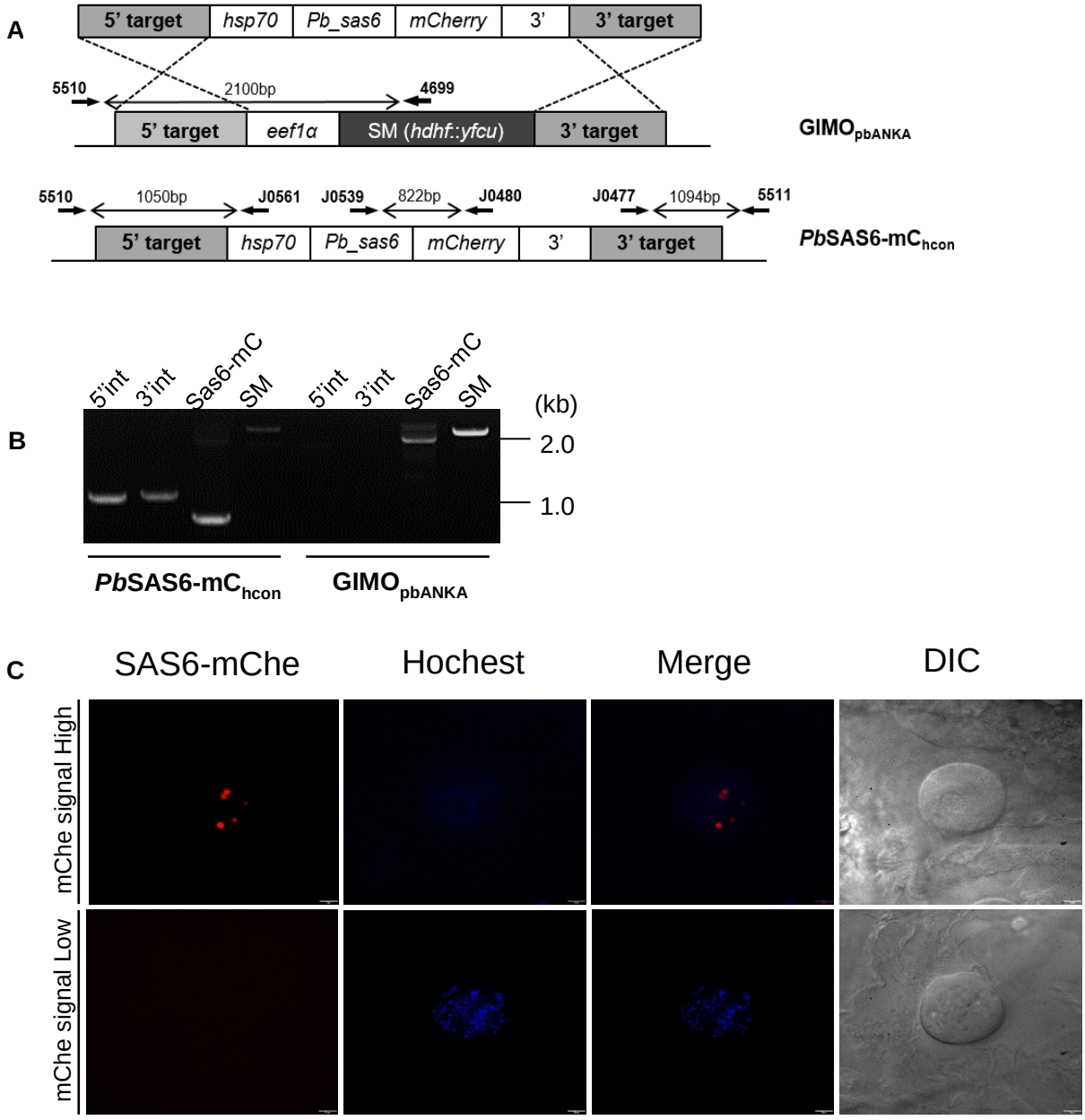
A
5' target
hsp70
Pb_sas6
mCherry
3'
3' target
5510
2100bp
4699
5' target
eef1α
SM (hdhf::yfcu)
3' target
GIMOpbANKA
5510
1050bp
J0561
J0539
822bp
J0480
J0477
1094bp
5511
5' target
hsp70
Pb_sas6
mCherry
3'
3' target
PbSAS6-mChcon
B
5'int
3'int
Sas6-mC
SM
5'int
3'int
Sas6-mC
SM
(kb)
2.0
1.0
PbSAS6-mChcon
GIMOpbANKA
C
SAS6-mChe
Hochest
Merge
DIC
mChe signal High
mChe signal Low

Movie 1

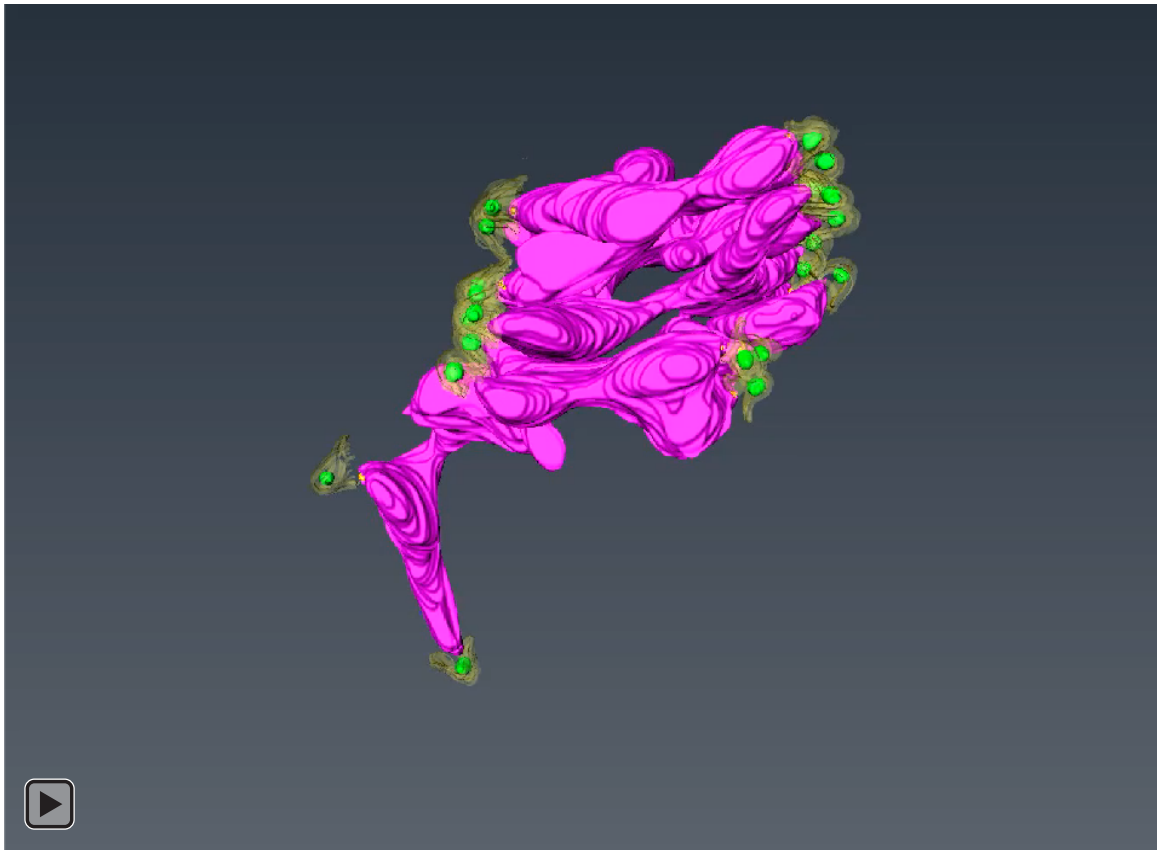

Movie 2

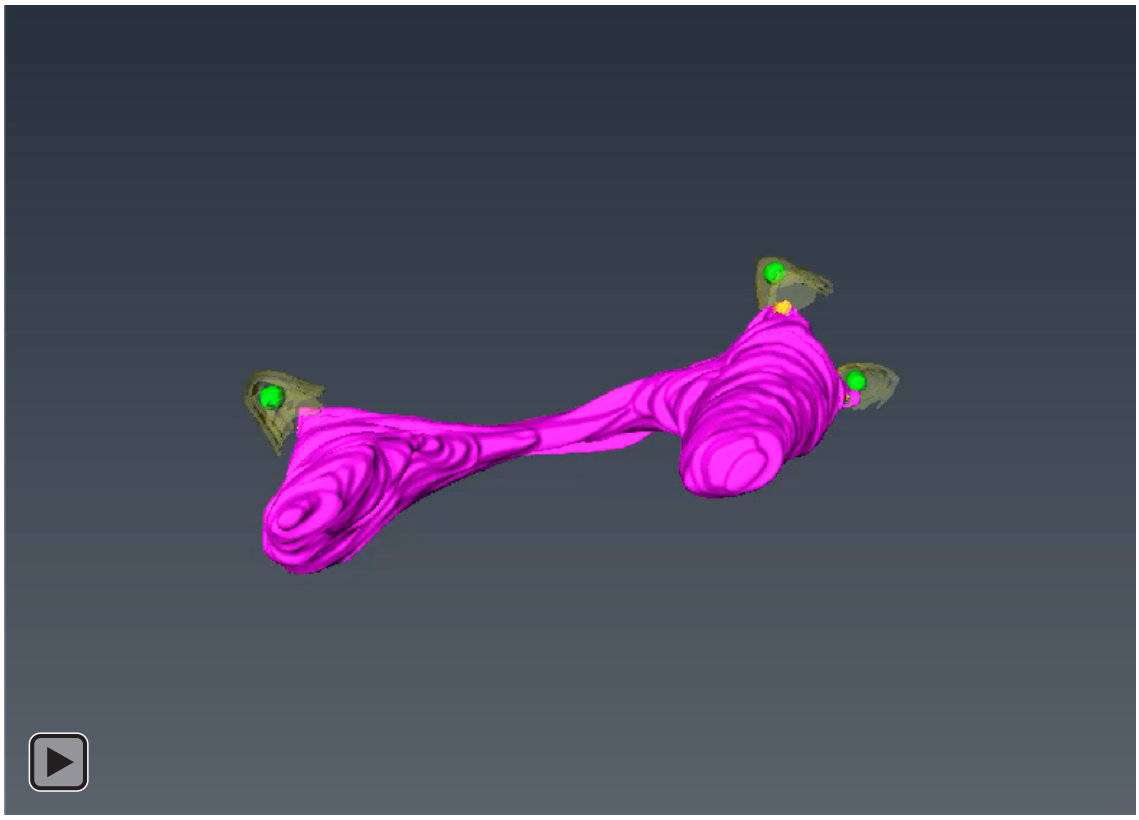

Movie 3

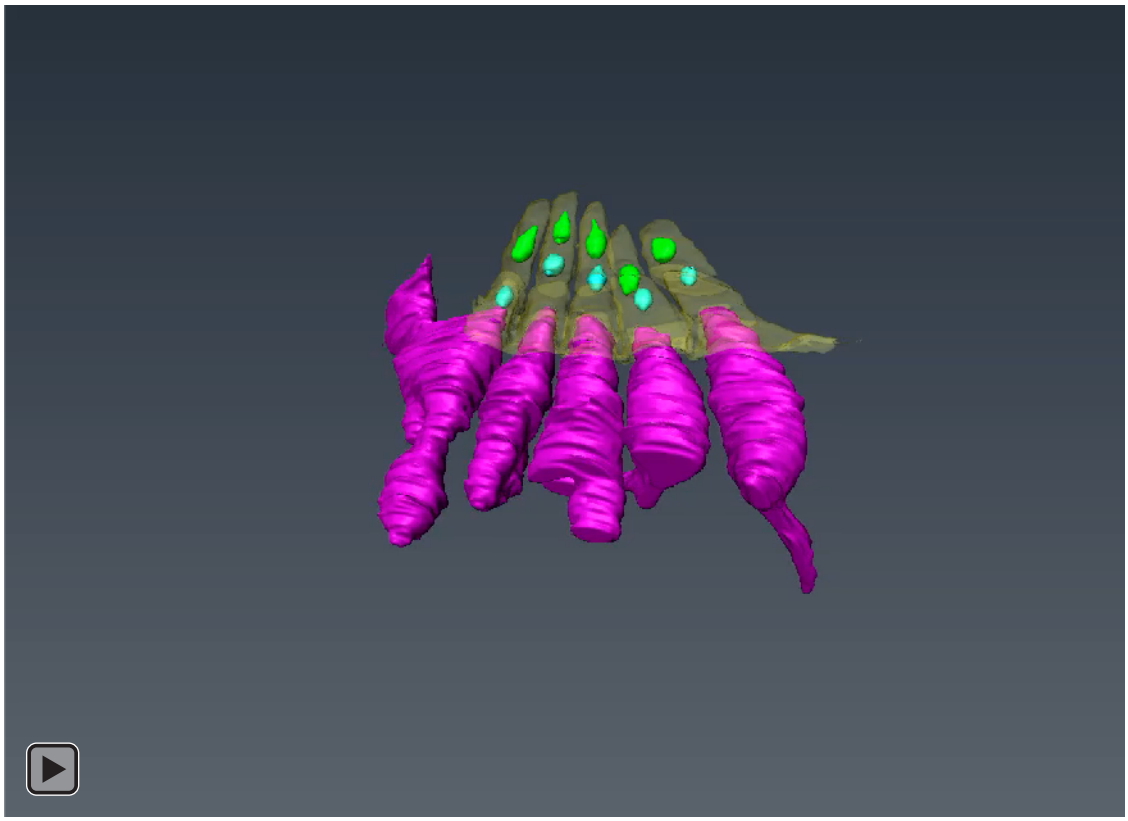

Movie 4

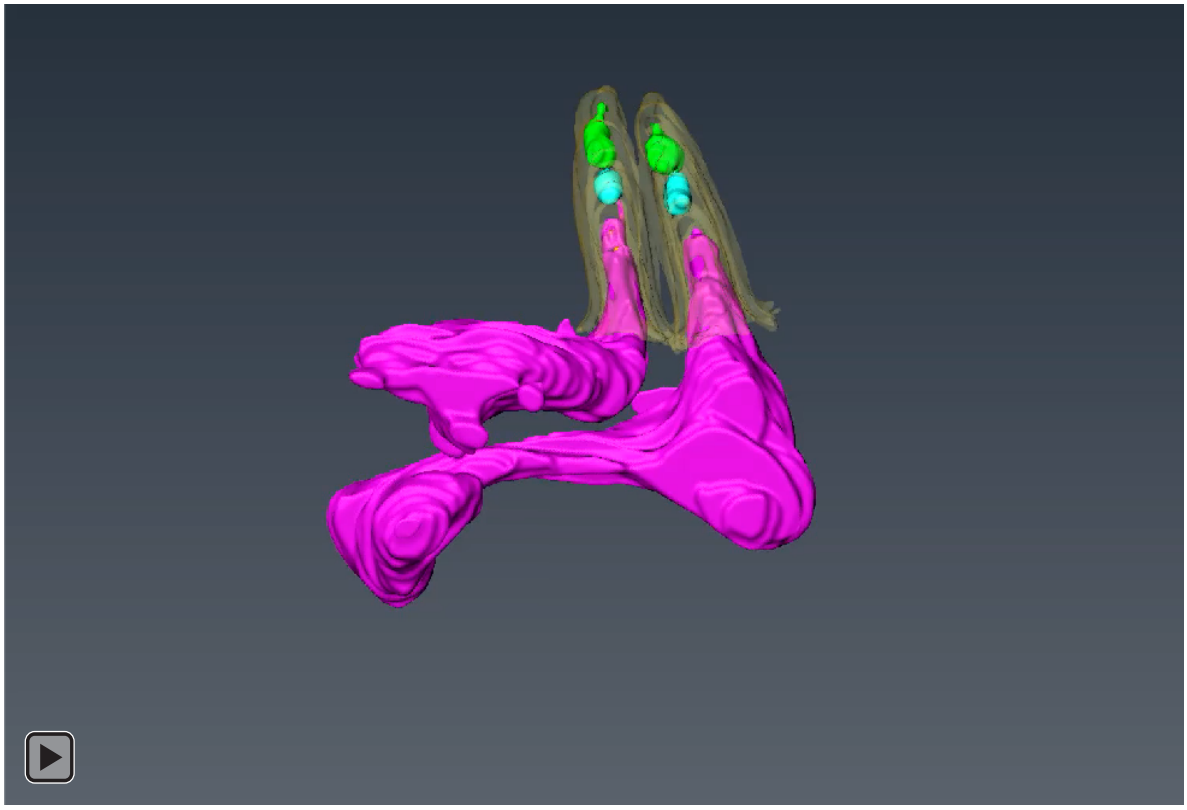

Movie 5

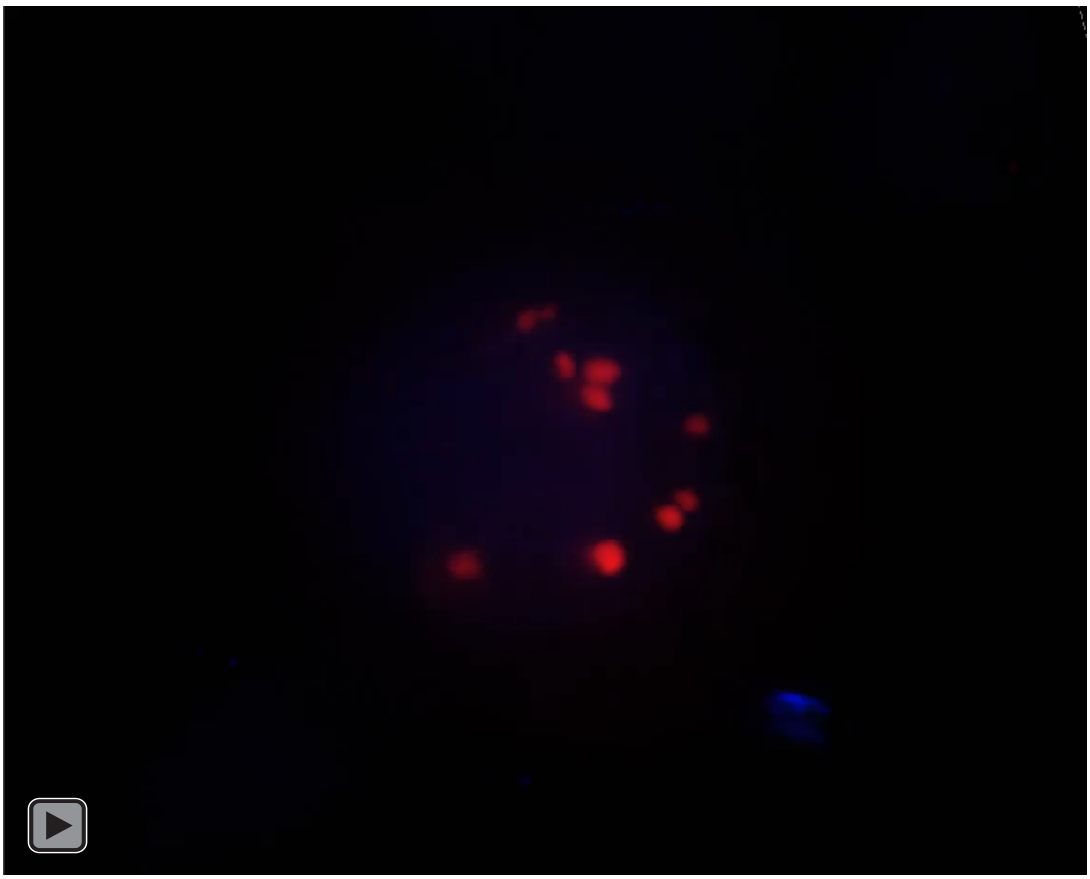

Movie 6

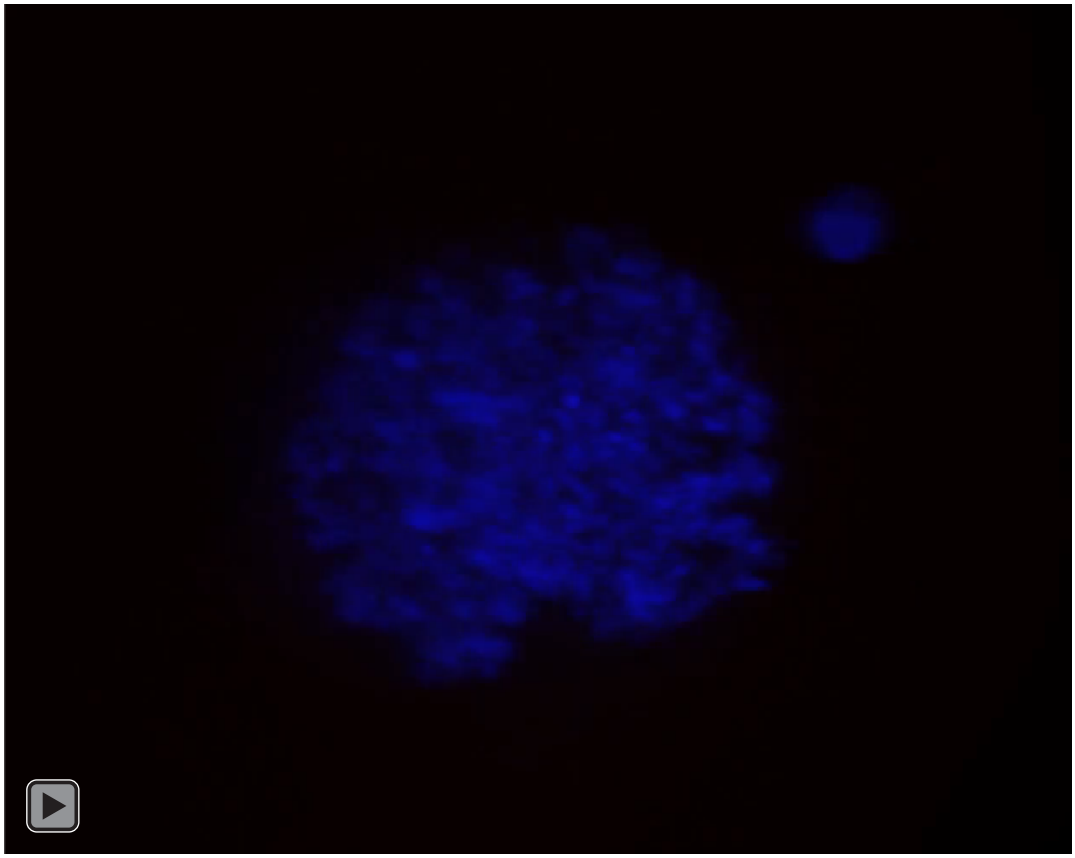

Table 2

Sequences of the primers used in this study.

	Name	Sequence	Description	Gene models
Primers for the generation of SAS6 (for PbSAS6-mC$_{hcon}$)				
Pb_sas6	J0632	tacaattacaattaaaaagATGAATTCGACGCACAATTATATC	Pb_sas6 F	PBANKA_0106200
Pb_sas6	J0633	cctcgcccttgctcaccatAATTCCGGGAGGAATAAATTTC	Pb_sas6 R	PBANKA_0106200
Primers for confirmation PCR of the integration event in PbSAS6-mC$_{hcon}$				
PbSAS6-mC$_{hcon}$	5510	GCAAAGTGAAGTTCAAATATGTG	PbSAS6-mC$_{hcon}$ 5' integration F	PBANKA_0306000
PbSAS6-mC$_{hcon}$	J0561	GTATGCACCCTTTGAGGGC	PbSAS6-mC$_{hcon}$ 5' integration R	PBANKA_0711900
PbSAS6-mC$_{hcon}$	J0477	AGACATGTTGTTATGCAAGTCTTTC	PbSAS6-mC$_{hcon}$ 3' integration F	PBANKA_0711900
PbSAS6-mC$_{hcon}$	5511	AGTGACTTTCAGTGAAATCGC	PbSAS6-mC$_{hcon}$ 3' integration R	PBANKA_0306000
PbSAS6-mC$_{hcon}$	J0539	CACACCAGCATACACATCAG	PbSAS6-mCherry F	PBANKA_0106200
PbSAS6-mC$_{hcon}$	J0480	CAGCTTCACCTTGTAGATG	PbSAS6-mCherry R	GIMO$_{pbANKA}$
PbSAS6-mC$_{hcon}$	5510	GCAAAGTGAAGTTCAAATATGTG	230P F	PBANKA_0306000
PbSAS6-mC$_{hcon}$	4699	GTTTGAGGTAGCAAGTAGACG	hdhfr::yfcu R	GIMO$_{pbANKA}$

Chapter 5. General discussion

Endopolygeny nuclear segregation that involves multiple rounds of DNA replication without nuclear division and internal budding within the cytoplasm has been observed in certain species of *Sarcocystis neurona* (Vaishnava et al., 2005) (Fig. 7). Nuclear division via both endodyogeny and endopolygeny has been reported in *Toxoplasma gondii* (Fig. 7). Endodyogeny is the formation of two daughters within the mother cell cytoplasm before the completion of nuclear division. *Toxoplasma* endopolygeny nuclear division was observed in the definitive host, which involved a proliferative phase with repeated nuclear division (Brooks et al., 2011; Nishi et al., 2008; Suvorova et al., 2015). A variety of nuclear division mechanisms are often found in these apicomplexan parasites according to the developmental stages, particularly during proliferation in the definitive or intermediate hosts. Considering that both endodyogeny and endopolygeny nuclear division mechanisms have been reported in intermediate and definitive *Toxoplasma* hosts, this could be related to haploid parasite generation. These observations suggested that the difference in proliferation systems occurred during the stage transition from diploid to haploid in the definitive host (Ferguson et al., 2007). However, the importance of endopolygeny formation in *Toxoplasma* remains under discussion.

My analysis revealed the endopolygeny-like nuclear architecture in the mosquito oocyst stage of *Plasmodium cynomolgi*, and this nuclear architecture was clearly different from the schizont stage that occurs in host blood. Therefore, the mechanisms of nuclear division in *Plasmodium* species might change according to the developmental stage. To reveal the nuclear division system in all stages of the *Plasmodium* life cycle, 3D FIB-SEM analysis needs to be performed on the liver stage of development. One of the most challenging questions is how to control nuclear segregation in *Plasmodium* at the liver stage, where the formation of dormant hypnozoites occurs. Therefore, the mechanism of nuclear regulation at the liver stage in *Plasmodium* species would be an attractive subject, particularly because it has been reported that the nucleus in hypnozoites remains as a single form during dormancy. However, because

of difficulties in setting up the hypnozoite stage of development, the number of hypnozoites would be limited. The targeting of hypnozoites for malaria elimination could shed light on a new strategy to discover novel antihypnozoite drugs that act via the mechanism of nuclear division in the future.

Acknowledgements

First of all I would like to express my gratitude to my supervisor, Dr. Takeshi Annoura (National Institute of Infectious Disease) for his helpful discussion and encouragements during the course of my work. I am grateful to Prof. Satoru Kawai (Dokkyo Medical University), Dr. Soichiro Kakuta (Juntendo University), Mr. Hirotaka Kobayashi (National Institute of Infectious Disease), Ms. Yuko Umeki (National Institute of Infectious Disease), Dr. Yumiko Saito-Nakano(National Institute of Infectious Disease), Dr. Toshinori Sasaki (National Institute of Infectious Disease), Dr. Yasuhiro Yasutomi (Tsukuba Primate Research Center), Prof. Tomoyoshi Nozaki (The University of Tokyo),Dr. Kumiko Nakada-Tsukui(National Institute of Infectious Disease), Dr. Blandine Franke-Fayard (Leiden University Medical Center), Dr. Shahid M. Khan(Leiden University Medical Center), Dr. Hajime Hisaeda (National Institute of Infectious Disease) for their technical assistance and valuable discussion. I would like to thank Dr.. Chris J Janse for kindly providing us *P. yoelii* 1971, *P. berghei* 676m1cl1 and GIMO parasites. The authors would also like to thank Ms. Sayuri Hasegawa and Ms. Ayako Arai for their help with the maintenance of Anopheles mosquitos, and Ms. Masako Takatsu for the plasmid DNA preparation. Finally, I thank all members of the laboratory of the Department of Parasitology (National Institute of Infectious Disease), and Graduate School of Medicine, the University of Tokyo.This research was partially supported by National Bio-Resource Project (NBRP) “Japanese Macaques” at Primate Research Institute, Kyoto University from Japan Agency for Medical Research and Development, AMED.

Reference

Annoura, T., Chevalley, S., Janse, C. J., Franke-Fayard, B., & Khan, S. M. (2013). Quantitative analysis of Plasmodium berghei liver stages by bioluminescence imaging. *Methods Mol Biol, 923*, 429-443. doi:10.1007/978-1-62703-026-7_30

Annoura, T., van Schaijk, B. C., Ploemen, I. H., Sajid, M., Lin, J. W., Vos, M. W., . . . Khan, S. M. (2014). Two Plasmodium 6-Cys family-related proteins have distinct and critical roles in liver-stage development. *Faseb j, 28*(5), 2158-2170. doi:10.1096/fj.13-241570

Aoki, K., Hayashi, H., Furuya, K., Sato, M., Takagi, T., Osumi, M., . . . Niki, H. (2011). Breakage of the nuclear envelope by an extending mitotic nucleus occurs during anaphase in Schizosaccharomyces japonicus. *Genes Cells, 16*(9), 911-926. doi:10.1111/j.1365-2443.2011.01540.x

Boettcher, B., & Barral, Y. (2014). The cell biology of open and closed mitosis. *Nucleus, 4*(3), 160-165. doi:10.4161/nucl.24676

Boettcher, B., Marquez-Lago, T. T., Bayer, M., Weiss, E. L., & Barral, Y. (2012). Nuclear envelope morphology constrains diffusion and promotes asymmetric protein segregation in closed mitosis. *The Journal of Cell Biology, 197*(7), 921-937. doi:10.1083/jcb.201112117

Brooks, C. F., Francia, M. E., Gissot, M., Croken, M. M., Kim, K., & Striepen, B. (2011). Toxoplasma gondii sequesters centromeres to a specific nuclear region throughout the cell cycle. *Proc Natl Acad Sci U S A, 108*(9), 3767-3772. doi:10.1073/pnas.1006741108

Canning, E. U., & Sinden, R. E. (1973). The organization of the ookinete and observations on nuclear division in oocysts of Plasmodium berghei. *Parasitology, 67*(1), 29-40. doi:10.1017/s0031182000046266

Cavalier-Smith, T. (2010). Origin of the cell nucleus, mitosis and sex: roles of intracellular coevolution. *Biol Direct, 5*, 7. doi:10.1186/1745-6150-5-7

Chang, F., & Martin, S. G. (2009). Shaping fission yeast with microtubules. *Cold Spring Harb Perspect Biol, 1*(1), a001347. doi:10.1101/cshperspect.a001347

Eshar, S., Dahan-Pasternak, N., Weiner, A., & Dzikowski, R. (2011). High resolution 3D perspective of Plasmodium biology: advancing into a new era. *Trends in Parasitology, 27*(12), 548-554. doi:10.1016/j.pt.2011.08.002

Ferguson, D. J. (2009). Toxoplasma gondii: 1908-2008, homage to Nicolle, Manceaux and Splendore. *Mem Inst Oswaldo Cruz, 104*(2), 133-148. doi:10.1590/s0074-02762009000200003

Ferguson, D. J., Campbell, S. A., Henriquez, F. L., Phan, L., Mui, E., Richards, T. A., . . . Roberts, C. W. (2007). Enzymes of type II fatty acid synthesis and apicoplast differentiation and division in Eimeria tenella. *Int J Parasitol, 37*(1), 33-51. doi:10.1016/j.ijpara.2006.10.003

Ferguson, D. J., Sahoo, N., Pinches, R. A., Bumstead, J. M., Tomley, F. M., & Gubbels, M. J. (2008). MORN1 has a conserved role in asexual and sexual development across the apicomplexa. *Eukaryot Cell, 7*(4), 698-711. doi:10.1128/EC.00021-08

Francia, M. E., & Striepen, B. (2014). Cell division in apicomplexan parasites. *Nat Rev Microbiol, 12*(2), 125-136. doi:10.1038/nrmicro3184

Gerald, N., Mahajan, B., & Kumar, S. (2011). Mitosis in the human malaria parasite Plasmodium falciparum. *Eukaryot Cell, 10*(4), 474-482. doi:10.1128/EC.00314-10

Ghebreyesus, T. A., & Admasu, K. (2018). Countries must steer new response to turn the malaria tide. *Lancet, 392*(10161), 2246-2247. doi:10.1016/s0140-6736(18)32943-x

Howells, R. E., & Davies, E. E. (1971). Nuclear division in the oocyst of Plasmodium berghei. *Ann Trop Med Parasitol, 65*(4), 451-459. doi:10.1080/00034983.1971.11686777

Kremer, A., Lippens, S., Bartunkova, S., Asselbergh, B., Blanpain, C., Fendrych, M., . . . Guerin, C. J. (2015). Developing 3D SEM in a broad biological context. *J Microsc, 259*(2), 80-96. doi:10.1111/jmi.12211

Kubai, D. F., & Ris, H. (1969). Division in the dinoflagellate Gyrodinium cohnii (Schiller). A new type of nuclear reproduction. *J Cell Biol, 40*(2), 508-528. doi:10.1083/jcb.40.2.508

Lin, J. W., Annoura, T., Sajid, M., Chevalley-Maurel, S., Ramesar, J., Klop, O., . . . Khan, S. M. (2011). A novel 'gene insertion/marker out' (GIMO) method for transgene expression and gene complementation in rodent malaria parasites. *PLoS One, 6*(12), e29289. doi:10.1371/journal.pone.0029289

Mahajan, B., Selvapandiyan, A., Gerald, N. J., Majam, V., Zheng, H., Wickramarachchi, T., . . . Kumar, S. (2008). Centrins, cell cycle regulation proteins in human malaria parasite Plasmodium falciparum. *J Biol Chem, 283*(46), 31871-31883. doi:10.1074/jbc.M800028200

Medeiros, L. C., De Souza, W., Jiao, C., Barrabin, H., & Miranda, K. (2012). Visualizing the 3D architecture of multiple erythrocytes infected with Plasmodium at nanoscale by focused ion beam-scanning electron microscopy. *PLoS One, 7*(3), e33445. doi:10.1371/journal.pone.0033445

Mitchison, T. J., & Salmon, E. D. (2001). Mitosis: a history of division. *Nat Cell Biol, 3*(1), E17-21. doi:10.1038/35050656

Nishi, M., Hu, K., Murray, J. M., & Roos, D. S. (2008). Organellar dynamics during the cell cycle of Toxoplasma gondii. *J Cell Sci, 121*(Pt 9), 1559-1568. doi:10.1242/jcs.021089

Perret, E., Davoust, J., Albert, M., Besseau, L., & Soyer-Gobillard, M. O. (1993). Microtubule organization during the cell cycle of the primitive eukaryote dinoflagellate Crypthecodinium cohnii. *J Cell Sci, 104 (Pt 3)*, 639-651.

Roques, M., Stanway, R. R., Rea, E. I., Markus, R., Brady, D., Holder, A. A., . . . Tewari, R. (2019). Plasmodium centrin PbCEN-4 localizes to the putative MTOC and is dispensable for malaria parasite proliferation. *Biol Open, 8*(1). doi:10.1242/bio.036822

Sakaguchi, M., Miyazaki, N., Fujioka, H., Kaneko, O., & Murata, K. (2016). Three-dimensional analysis of morphological changes in the malaria parasite infected red blood cell by serial block-face scanning electron microscopy. *J Struct Biol, 193*(3), 162-171. doi:10.1016/j.jsb.2016.01.003

Scholey, J. M., Brust-Mascher, I., & Mogilner, A. (2003). Cell division. *Nature, 422*(6933), 746-752.

doi:10.1038/nature01599

Schrevel, J., Asfaux-Foucher, G., Hopkins, J. M., Robert, V., Bourgouin, C., Prensier, G., & Bannister, L. H. (2008). Vesicle trafficking during sporozoite development in Plasmodium berghei: ultrastructural evidence for a novel trafficking mechanism. *Parasitology, 135*(Pt 1), 1-12. doi:10.1017/s0031182007003629

Shimoda, C. (2004). Forespore membrane assembly in yeast: coordinating SPBs and membrane trafficking. *J Cell Sci, 117*(Pt 3), 389-396. doi:10.1242/jcs.00980

Smoyer, C. J., & Jaspersen, S. L. (2014). Breaking down the wall: the nuclear envelope during mitosis. *Curr Opin Cell Biol, 26*, 1-9. doi:10.1016/j.ceb.2013.08.002

Striepen, B., Jordan, C. N., Reiff, S., & van Dooren, G. G. (2007). Building the perfect parasite: cell division in apicomplexa. *PLoS Pathog, 3*(6), e78. doi:10.1371/journal.ppat.0030078

Suvorova, E. S., Francia, M., Striepen, B., & White, M. W. (2015). A Novel Bipartite Centrosome Coordinates the Apicomplexan Cell Cycle. *PLOS Biology, 13*(3), e1002093. doi:10.1371/journal.pbio.1002093

Vaishnava, S., Morrison, D. P., Gaji, R. Y., Murray, J. M., Entzeroth, R., Howe, D. K., & Striepen, B. (2005). Plastid segregation and cell division in the apicomplexan parasite Sarcocystis neurona. *J Cell Sci, 118*(Pt 15), 3397-3407. doi:10.1242/jcs.02458

Weiner, A., Dahan-Pasternak, N., Shimoni, E., Shinder, V., von Huth, P., Elbaum, M., & Dzikowski, R. (2011). 3D nuclear architecture reveals coupled cell cycle dynamics of chromatin and nuclear pores in the malaria parasite Plasmodium falciparum. *Cell Microbiol, 13*(7), 967-977. doi:10.1111/j.1462-5822.2011.01592.x

White, N. J., Pukrittayakamee, S., Hien, T. T., Faiz, M. A., Mokuolu, O. A., & Dondorp, A. M. (2014). Malaria. *Lancet, 383*(9918), 723-735. doi:10.1016/s0140-6736(13)60024-0

Yam, C., He, Y., Zhang, D., Chiam, K. H., & Oliferenko, S. (2011). Divergent strategies for controlling the nuclear membrane satisfy geometric constraints during nuclear division. *Curr Biol, 21*(15), 1314-1319. doi:10.1016/j.cub.2011.06.052